Along arc heterogeneity in local seismicity across the Lesser Antilles subduction zone from a dense ocean-bottom seismometer network

Lidong Bie*, Andreas Rietbrock*, Stephen Hicks, Robert Allen, Jon Blundy, Valerie Clouard, Jenny Collier, Jon Davidson, Thomas Garth, Saskia Goes, Nick Harmon, Tim Henstock, Jeroen van Hunen, Mike Kendall, Frank Krüger, Lloyd Lynch, Colin Macpherson, Richard Robertson, Kate Rychert, Stephen Tait, Jamie Wilkinson, Marjorie Wilson

Corresponding author: Lidong Bie (l.bie@liv.ac.uk)
Geophysical Institute, Karlsruhe Institute of Technology, Germany
*Also at Department of Earth Ocean & Ecological Sciences, University of Liverpool, UK

ABSTRACT

The Lesser Antilles arc is only one of two subduction zones where slow-spreading Atlantic lithosphere is consumed. Slow-spreading may result in the Atlantic lithosphere being more pervasively and heterogeneously hydrated than fast-spreading Pacific lithosphere, thus affecting the flux of fluids into the deep mantle. Understanding the distribution of seismicity can help unravel the effect of fluids on geodynamic and seismogenic processes. However, a detailed view of local seismicity across the whole Lesser Antilles subduction zone is lacking. Using a temporary ocean-bottom seismic network we invert for hypocentres and 1-D velocity model. A systematic search yields a 27 km thick crust, reflecting average arc and back-arc structure. We find abundant intraslab seismicity beneath Martinique and Dominica, which may relate to the subducted Marathon/Mercurius Fracture Zones. Pervasive seismicity in the cold mantle wedge corner and thrust seismicity deep on the subducting plate interface suggest an unusually wide megathrust seismogenic zone reaching ~65 km depth. Our results provide an excellent framework for future understanding of regional seismic hazard in eastern Caribbean and the volatile cycling beneath the Lesser Antilles arc.

INTRODUCTION

Subduction zones are key centers of mass transfer in the Earth, where the lithosphere and its cargo of volatiles are recycled back into the Earth's interior. In contrast to Pacific subduction margins, where fast-spreading lithosphere is consumed, subduction of slow-spreading lithosphere such as that formed in the Atlantic should result in a more heterogeneous distribution and possibly higher amount of fluids entering the subduction zone (Escartín *et al.*, 2008). The Lesser Antilles subduction zone in Eastern Caribbean is a global end-member in that the subducting plate is relatively old (~80 Myr) but yet subducts very slowly at ~19 mm/yr (DeMets *et al.*, 2010), and it is one of two zones where the slow-spreading Atlantic oceanic lithosphere is consumed. Along-arc changes in fluid flux might affect the distribution and character of seismicity and associated volcanism. For example, pore fluids within subducting sediments may affect the seismic

character of subduction megathrusts (Heuret *et al.,* 2012), and intermediate-depth intraslab earthquakes are probably caused by dehydration embrittlement (e.g., Abers *et al.*, 2006). A coherent view of local seismicity throughout the Lesser Antilles subduction zone is thus important for understanding fluid pathways and their influence on seismicity as well as for improving seismic hazard assessment.

Available measurements for the Lesser Antilles arc indicate that subduction parameters, such as slab dip (Wadge and Shepherd, 1984), Wadati-Benioff zone thickness, and slab geometry (Bie et al., 2017), vary significantly along the Lesser Antilles subduction zone. Changes in slab dip as well as thickness and depth of the Wadati-Benioff zone near 15° latitude have been attributed to either the subduction of fracture zones (Schlaphorst *et al.*, 2016; Bie *et al.*, 2017) or a slab tear and gap wide enough to allow mantle flow through (e.g., van Benthem *et al.,* 2013; Harris *et al.*, 2018; Schlaphorst *et al.*, 2017). It is debated whether these changes in slab properties mark the location of the current North-South American plate boundary (Bie *et al.* 2017) or this boundary is located further north as suggested by plate reconstructions (Bird, 2003)

There have been several studies that characterise Lesser Antilles seismicity teleseismically (e.g., McCann and Sykes, 1984; Hayes *et al.*, 2013) as well as studies of local earthquakes for some parts of the arc (e.g., Dorel *et al.*, 1981; Paulatto *et al.*, 2017; Ruiz *et al.*, 2013). These studies found higher rates of seismicity in the northern part of the Lesser Antilles subduction zone (14-18° N) than in the south, both in terms of small events and in historical records (e.g., McCann and Sykes, 1984; Hayes *et al.*, 2013). Two historic M>8, presumably thrust, earthquakes have been documented in the northern Lesser Antilles (e.g., Feuillet *et al.*, 2011). However, the strength of plate interface coupling and its variation along strike remain uncertain due to sparse GPS observations and slow convergence (e.g., López *et al.*, 2006). Local studies have detected earthquakes in the fore-arc corner of the mantle wedge (Ruiz *et al.*, 2013, Laigle *et al.*, 2013), something that has only been seen in a few subduction zones worldwide (e.g., Halpaap *et al.*, 2019).

No recent efforts have systematically characterised the distribution of small-magnitude seismicity along the full extent of the Lesser Antilles plate margin. The inherent nature of oceanic subduction zones means that onshore permanent seismometer networks have limited coverage and aperture, making it difficult to accurately locate small-to-moderate magnitude earthquakes in the back- and fore-arc. Furthermore, there is no well-constrained 1-D velocity model for the Lesser Antilles, which adds to earthquake location uncertainties. As part of our Volatiles Recycling in the Lesser Antilles (VoiLA) project (Goes *et al.*, 2019), we deployed a network of 34 broadband ocean-bottom seismometers (OBS) in 2016, which were recording for 14 months. We use this OBS data, complemented by recordings from permanent and temporal land stations, to jointly invert for 1-D P- and S-wave velocity models, earthquake locations and station corrections. Our study provides the first unified reference velocity model for the Lesser Antilles region, useful for the routine location of earthquakes in the area. The recorded seismicity provides the opportunity to understand the fore- and back-arc structure, thermal structure in the mantle wedge, and deformation mechanisms at intermediate depths in the subducted slab.

SEISMIC EXPERIMENT AND DATA

In March 2016, a network of 34 broadband OBS was installed across the fore- and back-arc regions of the Lesser Antilles subduction zone (Figure 1). The OBS were retrieved in May 2017. Two stations encountered hardware failures, leaving 32 stations with useable data (Goes *et al.*, 2019). In addition to our temporal OBS observations, we collected seismic data from existing permanent stations as archived by IRIS DMC (Figure S1). We also filled the gap in permanent stations along the southern end of the arc by deploying eight temporary stations in January 2017.

Multi-channel seismic surveys were also made during expedition JC149 in April 2017. Shooting occurred along eight lines, most of which were in a north-south direction along the arc and in the back-arc, with two lines taken perpendicular to the arc in the north of the subduction zone (Figure S1). These active-source data help to constrain the shallow

velocity structure of the subduction zone, an area poorly resolved in many passive-source tomographic inversions.

MINIMUM 1-D VELOCITY MODEL

Initial Catalogue

By collating the events reported by various agencies, we created an initial earthquake catalogue for manual picking P- and S-wave onset times. Our initial catalogue includes events from the online bulletin of the International Seismological Centre (ISC), the Martinique Seismic and Volcano Observatory, and the Seismological Research Centre of the University of West Indies (hereafter, UWI-SRC). We also detected additional events using an automated short-term average ratio/long-term average (STA/LTA) triggering algorithm (Nippress *et al.,* 2010) on vertical components of the ocean-bottom stations and performed an iterative event association procedure following Rietbrock *et al.* (2012). We then manually read P- and S-wave onset times from these potential events on the ocean-bottom stations and all available onshore stations using the Seismic Data Explorer (SDX) software (http://doree.esc.liv.ac.uk:8080/sdx). Based on onset time uncertainties, we assigned each observation a weight as follows: Weight 0 (<0.1 s); Weight 1 (0.1-0.2 s); Weight 2 (0.2–0.5 s); Weight 3 (0.5–0.8 s); Weight 4 (>0.8 s). Initial locations were computed using the IASP91 1-D reference velocity model (Kennett and Engdahl, 1991). This workflow resulted in a total of 502 confirmed earthquakes.

We computed local magnitudes (M_L) for all events in our catalogue. Maximum amplitudes were taken from instrument-corrected waveforms, which were simulated to a Wood-Anderson seismometer. We took the largest peak-to-peak amplitude from all station components within a time window starting at the picked P-wave arrival and ending at a time window 30 seconds after the theoretical slowest travelling L_g wave (assuming a minimum L_g velocity of 3.0 km/s). We computed amplitudes for traces that had a root-mean square (RMS) signal-to-noise ratio greater than 3 to ensure that amplitude measurements were not contaminated by ocean microseism noise. We computed station magnitudes based on the M_L scale for central California (Bakun and

Joyner, 1984). Overall event magnitudes were then calculated based on a 25% trimmed-mean of station magnitudes to reject outliers. We found that station amplitudes measured at both ocean-bottom and onshore stations fit well the M_L scale over a range of hypocentral distance (see Figure S2 for examples). Regression analysis shows that our computed event local magnitudes correlate well with moment magnitude estimates for $M_w > 4.5$ events (Figure S3a), and with local duration magnitudes (M_d) for smaller events (Figure S3b).

1-D minimum velocity model inversion

Out of 502 manually picked events, we select a high-quality subset of 265 events with a maximum azimuthal gap of less than 180°, and with at least 20 P-wave and 5 S-wave arrivals. The subset consists of ~10,600 P-wave and ~8,200 S-wave arrivals for the simultaneous inversion of a 1-D layered velocity model, earthquake location and station corrections using the VELEST software (Kissling *et al.,* 1994).

The travel-time of a seismic wave is dependent on both the hypocentre parameters (origin time and location) and seismic velocity structure of the medium that the ray-path travels through. Such a coupled hypocentre-velocity problem can be solved by ray-tracing and updating the velocity model and hypocentre simultaneously (Kissling *et al.,* 1988; Eberhart-Phillips, 1990; Thurber, 1992). We conducted the simultaneous inversion using the VELEST software by Kissing *et al.* (1994). VELEST requires that all stations must be in the same velocity layer. In this study, the deepest OBS station sits ~5 km below sea level and the greatest land station elevation is ~1.4 km, making it impractical to set a model with a 7 km thick uppermost layer. Instead, we followed the strategy of Husen *et al.* (1999) and Hicks *et al.* (2014) by setting station elevations to zero and allowing station delay terms to absorb systematic travel-time errors due to elevation differences, as well as possible lateral heterogeneity in subsurface structure.

In addition to passive seismic data, we included 63 active shots from the seven shot lines (Figure 1) in order to better constrain seismic velocities at shallow depth, especially in the back-arc region, where few earthquakes with shallow hypocentral

depth occur. For each shot line, the gap between our selected neighbouring shots is roughly 15 km. The arrival times were manually picked on 22 OBS stations that record part of the 63 shots. The arrival times were corrected to subtract travel-time through the sea-water-column to be consistent with setting the station depth to sea level.

A robust initial starting velocity model is required as *a priori* information. We chose the velocity model computed by Raffaele (2011) as our starting model. Given that this model only extends to 30 km depth, we extended the starting model to a depth of 200 km by merging it with the IASP91 velocity model below 30 km depth. To search for the best-fitting minimum 1-D model, ensuring that we are not fitting local misfit minima, we perturbed the starting model randomly within ±0.5 km/s for all layers, resulting in 1000 different synthetic starting models. The degree of convergence of the final velocity models from the 1000 inversions with different starting models is the first evidence of how robust the best-fitting model is. The velocity model that gives the minimum root-mean-square (RMS) misfit was taken as the optimal minimum 1-D velocity model.

We first invert for P-wave velocity model, using P-wave arrivals only. The best 10 velocity models with the smallest RMS misfit converge very well. We notice an increase of velocity from 7.0 to 7.7 km/s at a depth of 27 km. To test whether the Moho depth can be constrained by our datasets, we manually alter the starting model by varying the depth to the bottom of the third layer from 21 to 37 km, in 2 km increments (Figure 2a). Then the inversion is conducted in the same way as described above by generating 1000 variations of starting models for each Moho depth scenario and searching for the best model that gives minimum RMS. We then plotted the minimum RMS values versus the prescribed Moho depths, and the comparison shows a preferred average Moho depth of 27 km (Figure 2c).

After obtaining the best P-wave velocity model and optimal Moho depth, we subsequently inverted for S-wave velocity model using P- and S-wave arrival times. Similarly, 1000 variations of S-wave starting velocity model are generated, based on the P-wave velocity model and average v_p/v_s ratio derived from Wadati analysis. Due to the

trade-off between station corrections and the top layer velocity, we chose not to fix the top layer P-wave velocity as derived from the inversion.

Characteristics of Minimum 1-D Velocity Model

Tests with a range of starting models with various Moho dept (Figure 2a) result in the final minimum 1-D velocity model shown in Figure 2b. The best-fitting 1-D minimum velocity model comprises two layers of upper-plate crust underlying a top sedimentary layer. The estimated crustal P-wave velocity increases from 4.3 km/s at shallow depth to 7.7 km/s at 27 km depth. Affected by mostly near-vertical ray-paths, the uppermost crustal layer velocity is less well constrained, shown by poor convergence of the 10 best models, implying strong spatial variation of uppermost crustal velocity. This does not influence the final earthquake locations however, as our analysis of locations corresponding to the best 10 velocity models show a small average shift of <100 meters in all directions. The average velocities for the two main crustal layers are 6.3 km/s and 7.0 km/s, consistent with those determined by Boynton *et al.* (1979) for the island arc. Our systematic search with varying crustal thickness yields a minimum misfit when the Moho depth is 27 km (Figure 2c). Crustal thicknesses derived by González *et al.* (2018) from surface wave and receiver function analysis under 19 land stations along the arc vary from 21 km beneath St Lucia to 33 km beneath Grenada in the south, with an average of 26 km (Figure 2c), which is similar to our model value even though this constitutes an average across the margin. Between 27 km and 200 km depth, the P-wave velocity (v_p) and S-wave velocity (v_s) increasing steadily to 8.7 km/s and 4.9 km/s, respectively, fits the observations (Table S1).

Station corrections are incorporated to compensate 3-D heterogeneity of near-surface velocity and station elevations. Station corrections for v_p are generally smaller than 0.5 s, while for v_s, the station corrections are larger but mostly below 1.0 s (Figure 3). There are some systematic patterns, including positive corrections (i.e., thicker or slower crust) north and negative corrections south of reference station DP05 near Martinique in the central arc, as well as a linear correlation between station elevation and correction for

the OBS (Figure S4). Based on active source imaging (Allen *et al.*, 2019), our preferred interpretation is a systematic variation in crustal thickness from north to south.

OVERALL CHARACTERISTICS OF LA SEISMICITY AND SUBDUCTION GEOMETRY

The best-fitting velocity model is used to relocate the original 502 manually-picked events. We conducted hypocentre location stability tests by randomly perturbing hypocentres ±7.5-12.5 km in 3-D, then relocating using the best-fitting 1-D velocity model (Figure 2b). When the azimuthal gap is less than ~270°, the earthquakes generally relocate back to their original positions (Figure 4a), with a standard deviation of 0.21, 0.17, and 0.77 km for latitude, longitude and depth, respectively (Figure 4b). In addition to the azimuthal gap, we retained events that were relocated within 5 km depth variation from the original position. Strict filtering after hypocentre location stability tests resulted in 378 well-relocated events (Figure 5).

Although our observation period is short, the relocated seismicity exhibits a higher rate in the northern part of the subduction zone than in the south (Figure 5 and 6), consistent with previous studies (e.g., Bie *et al.,* 2017). Sparse seismicity is observed in the forearc region within 50 km distance from the trench. However, station coverage close to the trench in the outer forearc is very limited, so detection and location accuracy here is reduced. Most seismicity beneath the outer forearc is found in the north, where the forearc is less wide, and OBS stations were closer to the trench. We note that more smaller earthquakes may be found using template-matching techniques (e.g., Zhu *et al*., 2019). Here, we focussed on the larger events with robust arrival time determination, particularly for the generation of a well-constrained 1-D seismic velocity, with less emphasis on the evolution of seismicity in time and space.

Seismicity extends from the shallow upper crust of the overriding plate to intermediate depths of 180 km in the central slab (Figure 5). The distribution of seismicity with depth displays two peaks (see inset to Figure 5). Shallow seismicity increases with depth and

reaches its first peak at ~25 km, stays relatively high until there is a sharp reduction below ~60 km depth. At depths greater than ~80 km, seismicity increases again to depth of 170 km. The shallow peak comprises events in the overlying arc crust, and between about 25 and 60 km depth, events along the plate interface and in the mantle wedge corner. The deep peak consists of events within the subducting slab. The depth ranges of these peaks are similar to those that Paulatto *et al.* (2017) identified below Martinique, who proposed that the peaks in mantle wedge and slab seismicity are associated with slab dehydration around 40 and 150 km depth. In Section 5 we discuss the seismicity in each part of the system in detail.

Our catalogue of regional seismicity provides new constraints on slab geometry. As shown in Figure 5, the seismicity distribution in this study does not agree well with the global Slab2 plate geometry model (Hayes *et al.*, 2018). The slab surface in Slab2 is up to 70 km shallower at depth of 180 km. Our seismicity is consistent with the teleseismically-constrained slab geometry of Bie *et al.* (2017) to ~80 km depth, while beyond that, seismicity in our study suggests a slightly steeper slab (profiles B-B', C-C', and D-D' in Figure S5). We thus integrated the local seismicity in this study with the global datasets used in Bie *et al.* (2017) and constructed a refined slab geometry (Figure 5). How the large difference in slab geometry affects geodynamic modelling and seismic hazard estimation will be a subject of a planned future study.

DISCUSSION

Earthquakes in the Overriding Plate

The shallow events lie in the overriding upper plate, reflecting fault failures in the fore-arc and/or are related to volcanic structures along the arc. Profile A-A' shows a cluster of events ~100 km westward of the trench at 14-25 km depth. These events are mostly aftershocks of the M_w 5.7 thrust earthquake on 17 April 2017. The trenchward-dipping alignment of the cluster may indicate failure of a back-thrust fault bounding the western edge of the accretionary prism. A similar cluster can be found ~150 km west of the trench in profile B-B'. It is unclear whether this cluster on B-B' was on splay thrusts or

back-thrusts, given no clear alignment is shown and the relatively large RMS misfit values.

Profile B-B' shows another cluster of shallow seismicity in line with the volcanic arc, between Guadeloupe and Dominica. This seismicity can be divided into two sequences. The first in 2016 starts with M_L 4.5 and M_L 4.1 events on 12 April, and lacks a clear subsequent aftershock sequence. The second sequence swarm started in April 2017 denoted by a M_L 3.5 earthquake (Table S2). Previously on 21 November 2004, this area experienced a M_w 6.3 normal fault earthquake on the Roseau fault, which bounds the western side of the Les Saintes Graben between Guadeloupe and Dominica (Bazin *et al.*, 2010). The mainshock was followed by a long-lasting aftershock sequence on the Roseau Fault and a short-lived aftershock sequence on the smaller antithetic normal faults. Bazin *et al.* (2010) attributed the long-lasting aftershock sequence on the Roseau fault to this region being strongly faulted and filled with fluids, as inferred from a low v_p anomaly and a high v_p/v_s ratio, while for the short duration aftershock sequence, fluid was less involved. This interpretation of high fluid content is consistent with our observation of occasional swarm activity in this region.

Below Tobago, in the southern fore-arc, a sequence of aftershocks followed the M_w 5.9 strike-slip earthquake on 6 December 2016 (profile E-E' of Figure 5). Although, we expected these to be upper plate events, the aftershocks were relocated to ~60 km depth. A M_w 6.1 earthquake with a similar faulting mechanism occurred on 2 April 1997 at 45 km depth (NEIC), preceding a larger M_w 6.7 normal fault earthquake on 22 April 1997 at a much shallower depth of 5-15 km (NEIC). The GCMT focal mechanism for the 2016 event suggests either sinistral strike-slip on an E-W striking sub-vertical (dip 67°) fault plane, or dextral strike-slip rupture on a near-vertical (80° dip) N-S striking fault (Figure 6). This mechanism is not consistent with the current active E-W dextral shearing across the Caribbean-South American plate boundary zone (e.g., Weber *et al.*, 2015). These strike-slip events lie anomalously deep beneath the fore-arc, and the 2016 cluster is close to the top of the subducting slab (profile E-E' of Figure 5). A likely

explanation is that the 2016 and 1997 strike-slip events ruptured structures within the down-going oceanic crust.

Mantle Wedge Seismicity

In addition to shallow upper crust activity, seismicity in the overriding plate appears in the mantle wedge corner above ~65 km depth and reaches into the lower crust (profiles in Figure 5), consistent with Ruiz *et al.* (2013) and Laigle *et al.* (2013). Seismicity in the mantle-wedge corner has implications for the thermal structure of the mantle wedge. It is normally assumed that the stable-unstable sliding transition in oceanic mantle occurs at temperatures of ~600°C (e.g., McKenzie *et al.,* 2005). By constructing an approximate curve delineating the wedge-shaped mantle corner seismicity, we found that the inferred transition consistently intersects the slab (red curve constrained by seismicity in Figure 5 profiles) at ~65 km depth across the subduction zone. In contrast to profiles in the north, the lack of mantle wedge seismicity in the EE' profile suggests that the mantle wedge temperature is different from north to south.

Mantle-wedge corner seismicity has been reported in only a few subduction zones around the world besides the Antilles, namely, NE Japan, New Zealand, Columbia and Greece. Such events have been attributed to the deformation of subducted seamounts (Uchida *et al.,* 2010), or hydraulic fracturing/fluid-assisted embrittlement or weakening due to the ascent of fluids from the slab (Chang *et al.*, 2017, Halpaap *et al.,* 2019). If this is the case for the Lesser Antilles, then the mantle wedge earthquakes may represent an unusual pathway for fluids driven off by early metamorphic reactions in the subducting plate. Alternatively, in a mantle wedge of mixed chemical composition (Laigle et al., 2013), preferential hydration of the peridotite components may result in a differential volume change that may open fractures, causing extensional faulting in the mantle wedge (Iyer et al., 2008).

Plate Interface Seismicity

In the north, interplate seismicity is observed from depths of about 10 km, while in the south, the shallowest seismicity is at 30 km depth at 14°N, and 45 km south of 12°N

(profiles in Figure 5). The largest thrust earthquake (M_w 5.8) on the plate interface during our deployment occurred on 3 February 2017 east of Martinique. The Martinique earthquake was followed by aftershocks at ~50 km depth (profile C-C'). We relocated the M_w 5.8 mainshock to 51 km depth. The alignment of the sequence with the slab geometry indicates rupture of the plate interface and suggests a seismogenic zone reaching to at least 60 km depth, deeper than the fault locking depth of 5-25 km previously proposed by Symithe *et al.* (2015) using geodetic observations.

The Martinique sequence occurred deeper than the intersection of the upper plate Moho (~27 km) with the down-going plate interface. This observation is similar to that found by Ruiz *et al.* (2013) of seismic activity offshore Martinique and Dominica, suggesting that the interplate seismogenic zone width is usually not limited by thickness of the upper plate crust, consistent with a global compilation by Heuret *et al.* (2011). However, the down-dip limit of ~65 km depth that we find for the Lesser Antilles megathrust seismogenic zone is high compared to the global range of 51±8 km (Heuret *et al.,* 2011). The Martinique sequence on the plate interface, together with supra-slab seismicity discussed in the previous section, suggest the existence of a cold mantle nose, which can effectively extend the decoupling depth of the slab and upper plate mantle (Wada and Wang, 2009). This wide seismogenic zone has important implications for the maximum magnitude of earthquakes that could occur in this region, and this may explain the large magnitudes of the Guadeloupe earthquakes in the 1800s. An alternative to this is that this deeper part may represent seismic-aseismic transitional zone (e.g., Lay et al., 2012). Although large earthquakes may not initiate at this deeper depth, rupture may propagate into this region and effectively increase the earthquake magnitude and thus seismic hazard.

Intermediate Depth Seismicity

The Lesser Antilles Wadati-Benioff zone extends to 150-180 km depth with a concentration of intraslab seismicity beneath the center of the arc, between the islands of Guadeloupe and St. Lucia (Figure 5). During our experiment, a M_w 5.6 earthquake occurred on 18 October 2016 southwest of Dominica at ~160 km depth. This event had

a normal faulting mechanism with both nodal planes striking perpendicular to the arc, and in the direction of convergence. Normal faulting earthquakes are frequent within the slab at ~150 km depth between the islands of Dominica and Martinique, i.e. in the region with the densest intermediate depth seismicity. Similar recent moderate-to-large intraplate events (Figure 6) include a M_w 5.6 on 28 December 2015, a M_w 7.4 on 29 November 2007, and a M_w 5.8 on 24 September 1996 and an earlier magnitude 7.5 that occurred on 19 March 1953 (Stein *et al.*, 1983) ~100 km south of the 2016 event. According to the GCMT earthquake catalogue, all those events since the 1990s share a similar, normal faulting mechanism with a minor strike-slip component; at least one of the nodal planes strikes parallel with the subduction direction.

Fault strikes parallel or oblique to the trench could be due to reactivation of subducted outer-rise normal faults formed at the mid-oceanic spreading ridge (e.g., Delouis and Legrand, 2007; Garth and Rietbrock, 2014). However, trench-perpendicular nodal plane ruptures cannot be explained in this manner. Instead, the intermediate-depth normal fault earthquakes mentioned above occurred around the projected positions of the subducted Marathon and Mercurius Fracture zones (Figure 6). This finding may suggest a link between the deep normal fault earthquakes and subducted fracture zones – which may be effective vessels to bring water to intermediate depths. Thus, the reactivation of inherited oceanic structures (e.g., fractures zones), facilitated by dehydration embrittlement, may be the dominant mechanism responsible for the normal faulting events seen at intermediate depth in the central arc. In other places along the arc, intermediate depth normal fault earthquakes are rare, which may suggest weaker hydration and smaller fluid fluxes, insufficient to drive significant dehydration embrittlement failure.

Slab Tear?

The coherent catalogue of seismicity compiled for this study offers a chance to test the hypothesis that a slab tear exists at 15°N - between the islands of Dominica and Martinique – as suggested by teleseismic tomography models and seismic anisotropy observations (Van Benthem *et al.,* 2013; Harris *et al.,* 2018; Schlaphorst *et al.,* 2017).

We projected seismicity in this area onto multiple profiles (with a 10 km gap between neighbouring profiles) perpendicular to the trench and marked those to the north of the profile in blue, and those to the south in red (Figure S6). This method can reveal the location of a slab tear, if two seismicity alignments with different dip angles are observed. Our results do not indicate any distinctive change in dip angle but rather a thickening of the Wadati-Benioff zone from north to south as shown by line 7 in Figure S6. The thickening here may define the northern boundary of the subducted Marathon Fracture zone. Seismicity during the period of our observation does not support the notion that a large-scale slab tear exists at this depth, but we cannot rule out a slab tear below the deepest seismicity.

CONCLUSIONS

In this study, we used seismic data from a dense OBS network to record local seismicity in the Lesser Antilles subduction zone and delineate changes in seismic deformation and velocity structure both with depth and along the arc. The joint inversion for a 1-D velocity model, earthquake location and station corrections yields an optimal crustal thickness of 27 km, representative of an arc-back-arc average. Abundant intermediate-depth seismicity is found beneath the islands of Martinique and Dominica, which may relate to the subducted Marathon and Mercurius Fracture Zones. Although a slab tear near 15°N has been proposed by previous teleseismic seismic studies, our seismicity distribution suggests thickening of the Wadat-Benioff zone, but without distinctive changes in the slab dip angle that would be expected for a tear. Interpretations of our earthquake locations reveal pervasive seismicity in the cold mantle wedge corner, which is not observed in many subduction zones. Together with the deep 2016 Martinique earthquake sequence on the plate interface, these observations suggest an abnormally cold and, therefore, wide megathrust seismogenic zone reaching ~65 km depth. It is worth to further investigate whether these features are inherent to the slow subduction of slow-spreading oceanic lithosphere in the Atlantic. These results provide a new framework for advances in operational earthquake locations and future estimation of seismic hazard in the Eastern Caribbean.

DATA AND RESOURCES

The optimal 1-D velocity model is made available in the electronic supplement to this article (Table S1). The relocated earthquake catalogue is available in Table S2. The Global Centroid Moment Tensor Project database was searched using www.globalcmt.org/CMTsearch.html (last accessed on April 1, 2019). We made figures using GMT (Wessel and Smalley, 1998). Supplemental content for this article includes figures showing the quality of earthquake magnitude estimation, the relationship between station correction and elevation, the comparison of our slab geometry with that of Slab2.0, and seismicity projected to dense profiles in the central part of the arc.

ACKNOWLEDGEMENTS

This work was funded under NERC grant NE/K010611/1. We thank the “German Instrument Pool for Amphibian Seismology (DEPAS)”, hosted by the Alfred Wegener Institute Bremerhaven, for providing the ocean-bottom seismometers and temporary island seismometers, and UCSD (Scripps) for providing additional ocean-bottom seismometers. We thank Allison Bent, Zhigang Peng, Hongfeng Yang, and two anonymous reviewers for their helpful and constructive comments.

REFERENCES

Allen, R., J. Collier, T. Henstock, A. Stewart, and S. Goes, 2019, A new tectonic model for the Lesser Antilles: Evidence for a buried arc in the eastern Caribbean, Geophysical Research Abstract, 21, EGU2019-7944

Bakun, W. H., and W. B., Joyner (1984), The ML scale in central California, Bull. Seismol. Soc. Am.,74(5), 1827-1843.

Bie, L., T. Garth, and A. Rietbrock, 2017, Links between the distribution of intermediate depth seismicity and structure of the incoming plate in the Lesser Antilles arc, In AGU Fall Meeting Abstracts. #T31D-0672

Abers, G. A., P. E. van Keken, E. A. Kneller, A. Ferris, and J. C. Stachnik (2006), The thermal structure of subduction zones constrained by seismic imaging: Implications for slab dehydration and wedge flow, Earth Planet. Sci. Lett., 241(3-4), 387-397.

Bazin, S., N. Feuillet, C. Duclos, W. Crawford, A. Nercessian, M. Bengoubou-Valérius, et al., (2010), The 2004–2005 Les Saintes (French West Indies) seismic aftershock sequence observed with ocean bottom seismometers, Tectonophysics, 489(1-4), 91-103.

Bird, P. (2003), An updated digital model of plate boundaries, Geochem. Geophys. Geosyst., 4(3), 1027, doi:10.1029/2001GC000252.

Boynton, C. H., G. K. Westbrook, M. H. P. Bott, and R. E. Long (1979), A seismic refraction in- vestigation of crustal structure beneath the Lesser Antilles islanc arc, Geophys. J. R. Astron. Soc., 58, 371–393.

Chang, Y., L. M. Warren, and G. A. Prieto (2017), Precise Locations for Intermediate-Depth Earthquakes in the Cauca Cluster, Colombia, Bull. Seismol. Soc. Am., 107(6), 2649-2663.

Delouis, B., and D. Legrand (2007), Mw 7.8 Tarapaca intermediate depth earthquake of 13 June 2005 (northern Chile): Fault plane identification and slip distribution by waveform inversion, Geophys. Res. Lett., 34(1).

DeMets, C., R. G. Gordon, and D. F. Argus (2010), Geologically current plate motions, Geophys. J. Int., 181, 1–80.

Dorel, J. (1981), Seismicity and seismic gap in the Lesser Antilles arc and earthquake hazard in Guadeloupe, Geophys. J. R. Astron. Soc., 67(3), 679-695.

Eberhart-Phillips, D. (1990), Three-dimensional P and S velocity structure in the Coalinga region, California. J. Geophys. Res., 95(B10), 15343-15363.

Escartín, J., D. K. Smith, J. Cann, H. Schouten, C. H. Langmuir, and S. Escrig (2008), Central role of detachment faults in accretion of slow-spreading oceanic lithosphere, Nature, 455(7214), 790.

Feuillet, N., F. Beauducel, and P. Tapponnier (2011), Tectonic context of moderate to large historical earthquakes in the Lesser Antilles and mechanical coupling with volcanoes, J. Geophys. Res., 116(B10), doi:10.1029/2011JB008443

Garth, T., and A. Rietbrock (2014), Downdip velocity changes in subducted oceanic crust beneath Northern Japan-insights from guided waves, Geophys. J. Int., 198(3), 1342-1358. doi:10.1093/gji/ggu206

González, O., V. Clouard, and J. Zahradnik (2017), Moment tensor solutions along the central Lesser Antilles using regional broadband stations, Tectonophysics, 717, 214-225.

González, O., V. Clouard, S. Tait, and G. F. Panza (2018), S-wave velocities of the lithosphere-asthenosphere system in the Lesser Antilles from the joint inversion of surface wave dispersion and receiver function analysis, Tectonophysics, 734, 1-15.

Halpaap, F., S. Rondenay, A. Perrin, S. Goes, L. Ottemöller, H. Austrheim, R. Shaw, and T. Eeken (2019), Earthquakes track subduction fluids from slab source to mantle wedge sink, Sci. Adv., 5(4), DOI: 10.1126/sciadv.aav7369.

Harris, C. W., M. S. Miller, and R. W. Porritt (2018), Tomographic Imaging of Slab Segmentation and Deformation in the Greater Antilles, Geochem. Geophys. Geosyst.,

Hayes, G. P., D. E. McNamara, L. Seidman, and J. Roger (2013), Quantifying potential earthquake and tsunami hazard in the Lesser Antilles subduction zone of the Caribbean region, Geophys. J. Int., 196(1), 510-521.

Hayes, G. P., G. L. Moore, D. E. Portner, M. Hearne, H. Flamme, M. Furtney, and G. M. Smoczyk (2018), Slab2, a comprehensive subduction zone geometry model, Science, 362(6410), 58-61.

Heuret, A., C. P. Conrad, F. Funiciello, S. Lallemand, and L. Sandri (2012), Relation between subduction megathrust earthquakes, trench sediment thickness and upper plate strain, Geophys. Res. Lett., 39(5).

Heuret, A., S. Lallemand, F. Funiciello, C. Piromallo, and C. Faccenna (2011), Physical characteristics of subduction interface type seismogenic zones revisited, Geochem. Geophys. Geosyst.,12(1).

Hicks, S., A. Rietbrock, I. Ryder, C. Lee, and M. Miller (2004), Anatomy of a megathrust: The 2010 M8.8 Maule, Chile earthquake rupture zone imaged using seismic tomography, Earth Planet. Sci. Lett., 405, 142-155, doi.org/10.1016/j.epsl.2014.08.028

Husen, S., E. Kissling, E. Flueh, and G. Asch (1999), Accurate hypocentre determination in the seismogenic zone of the subducting Nazca Plate in northern Chile using a combined on/offshore network, Geophys. J. Int., 138(3), 687-701.

Iyer, K., B. Jamtveit, J. Mathiesen, A. Malthe-Sørenssen, and J. Feder (2008), Reaction-assisted hierarchical fracturing during serpentinization, Earth Planet. Sci. Lett., 267(3-4), 503-516.

Kennett B. L. N., and E. R. Engdahl (1991), Travel times for global earthquake location and phase association, Geophys. J. Int., 105, 429-465.

Kissling, E., W. L. Ellsworth, D. Eberhart-Phillips, and U. Kradolfer (1994), Initial reference models in local earthquake tomography, J. Geophys. Res., 99, 19,635–19,646, doi:10.1029/93JB03138.

Kissling, E. (1988), Geotomography with local earthquake data, Rev. Geophys., 26(4), 659-698.

Laigle, M., A. Hirn, M. Sapin, A. Bécel, P. Charvis, E. Flueh, et al., (2013), Seismic structure and activity of the north-central Lesser Antilles subduction zone from an integrated approach: Similarities with the Tohoku forearc, Tectonophysics, 603, 1-20.

Lay, T., H. Kanamori, C. J. Ammon, K. D. Koper, A. R. Hutko, L. Ye, H. Yue, and T. M. Rushing (2012), Depth-varying rupture properties of subduction zone megathrust faults. J. Geophys. Res., 117(B4311), doi:10.1029/2011JB009133.

López, A. M., S. Stein, T. Dixon, G. Sella, E. Calais, P. Jansma, Weber, and P. LaFemina (2006), Is there a northern Lesser Antilles forearc block?, Geophys. Res. Lett., 33(7).

McCann, W. R., and L. R. Sykes (1984), Subduction of aseismic ridges beneath the Caribbean plate: Implications for the tectonics and seismic potential of the northeastern Caribbean, J. Geophys. Res., 89(B6), 4493-4519.

McKenzie, D., J. Jackson, and K. Priestley (2005), Thermal structure of oceanic and continental lithosphere, Earth Planet. Sci. Lett., 233(3-4), 337-349.

Nippress, S. E. J., A. Rietbrock, and A. E. Heath (2010), Optimized automatic pickers: application to the ANCORP data set. Geophys. J. Int., 181(2), 911-925.

Paulatto, M., M. Laigle, A. Galve, P. Charvis, M. Sapin, G. Bayrakci, ... and H. Kopp (2017), Dehydration of subducting slow-spread oceanic lithosphere in the Lesser Antilles, Nat. Comm., 8, 15980.

606 Raffaele, R. M. (2011), Seismic structure of subduction zone of the Lesser Antilles, PhD
607 thesis, University of Catania.
608
609 Rietbrock, A., I. Ryder, G. Hayes, C. Haberland, D. Comte, S. Roecker, and H. Lyon-
610 Caen (2012), Aftershock seismicity of the 2010 Maule Mw8.8, Chile, earthquake:
611 Correlation between co-seismic slip models and aftershock distribution? Geophys. Res.
612 Lett., 39(8). doi:10.1029/2012GL051308.
613
614 Ruiz, M., A. Galve, T. Monfret, M. Sapin, P. Charvis, M. Laigle, ... and J. Diaz (2013),
615 Seismic activity offshore Martinique and Dominica islands (Central Lesser Antilles
616 subduction zone) from temporary onshore and offshore seismic networks,
617 Tectonophysics, 603, 68-78.
618
619 Goes, S., et al. (2019), Project VoiLA: Volatile Recycling in the Lesser Antilles, Eos,
620 100, https://doi.org/10.1029/2019EO117309.
621
622 Schlaphorst, D., J. M. Kendall, J. S. Collier, J. P. Verdon, J. Blundy, B. Baptie, ... and M.
623 P. Bouin (2016), Water, oceanic fracture zones and the lubrication of subducting plate
624 boundaries—insights from seismicity, Geophys. J. Int., 204(3), 1405-1420.
625
626 Schlaphorst, D., J. M. Kendall, B. Baptie, J. L. Latchman, and S. Tait (2017), Gaps,
627 tears and seismic anisotropy around the subducting slabs of the Antilles,
628 Tectonophysics, 698, 65-78.
629
630 Stein, S., J. F. Engeln, D. A. Wiens, R. C. Speed, and K. Fujita (1983), Slow subduction
631 of old lithosphere in the Lesser Antilles, Tectonophysics, 99(2-4), 139-148.
632
633 Symithe, S., E. Calais, J. B. De Chabalier, R. Robertson, and M. Higgins (2015),
634 Current block motions and strain accumulation on active faults in the Caribbean, J.
635 Geophys. Res., 120(5), 3748-3774.
636
637 Thurber, C. H. (1992), Hypocenter-velocity structure coupling in local earthquake
638 tomography, Phys. Earth Planet. In., 75(1-3), 55-62.
639
640 Uchida, N., S. H. Kirby, T. Okada, R. Hino, and A. Hasegawa (2010), Supraslab
641 earthquake clusters above the subduction plate boundary offshore Sanriku,
642 northeastern Japan: Seismogenesis in a graveyard of detached seamounts?, J.
643 Geophys. Res., 115(B9).
644
645 van Benthem, S., R. Govers, W. Spakman, and R. Wortel (2013), Tectonic evolution
646 and mantle structure of the Caribbean, J. Geophys. Res., 118(6), 3019-3036.
647
648 Wada, I., and K. Wang (2009), Common depth of slab-mantle decoupling: Reconciling
649 diversity and uniformity of subduction zones, Geochem. Geophys. Geosyst., 10(10).
650

651 Wadge, G., and J. B. Shepherd (1984). Segmentation of the Lesser Antilles subduction
652 zone, Earth Planet. Sci. Lett., 71(2), 297-304.
653
654 Weber, J. C., H. Geirsson, J. L. Latchman, K. Shaw, P. La Femina, S. Wdowinski, et al.,
655 (2015), Tectonic inversion in the Caribbean-South American plate boundary: GPS
656 geodesy, seismology, and tectonics of the Mw 6.7 22 April 1997 Tobago earthquake,
657 Tectonics, 34(6), 1181-1194.
658
659 Wessel, P., and R. Smalley (1998). New, improved version of generic mapping tools
660 released, Eos Trans. AGU 79, no. 47, 579-579.
661
662 Zhu, G., H. Yang, J. Lin, Z. Zhou, M. Xu, J. Sun, and K. Wan (2019), Along-strike
663 variation in slab geometry at the southern Mariana subduction zone revealed by
664 seismicity through ocean bottom seismic experiments, Geophys. J. Int., 218(3), 2122-
665 2135, doi:10.1093/gji/ggz272.

Lidong Bie
Andreas Rietbrock
Geophysical Institute, Karlsruhe Institute of Technology, Germany
Department of Earth Ocean & Ecological Sciences, University of Liverpool, UK
l.bie@liv.ac.uk

Stephen Hicks
Robert Allen
Jenny Collier
Saskia Goes
Department of Earth Science & Engineering, Imperial College London, UK

Jon Blundy
Mike Kendall
School of Earth Sciences, University of Bristol, UK

Nick Harmon
Tim Henstock
Kate Rychert
Department of Ocean & Earth Sciences, University of Southampton, UK

Jon Davidson(Deceased)
Colin Macpherson
Jeroen van Hunen
Department of Earth Sciences, University of Durham, UK

Valerie Clouard
Stephen Tait
Institut de Physique du Globe de Paris, Université Paris Diderot, France

Thomas Garth

Department of Earth Sciences, University of Oxford, UK

Lloyd Lynch
Richard Robertson
Seismic Research Centre, The University of the West Indies, Trinidad and Tobago

Frank Krüger
Institute of Geosciences, University of Potsdam, Germany

Jamie Wilkinson
Natural History Museum, London, UK

Marjorie Wilson
School of Earth & Environment, University of Leeds

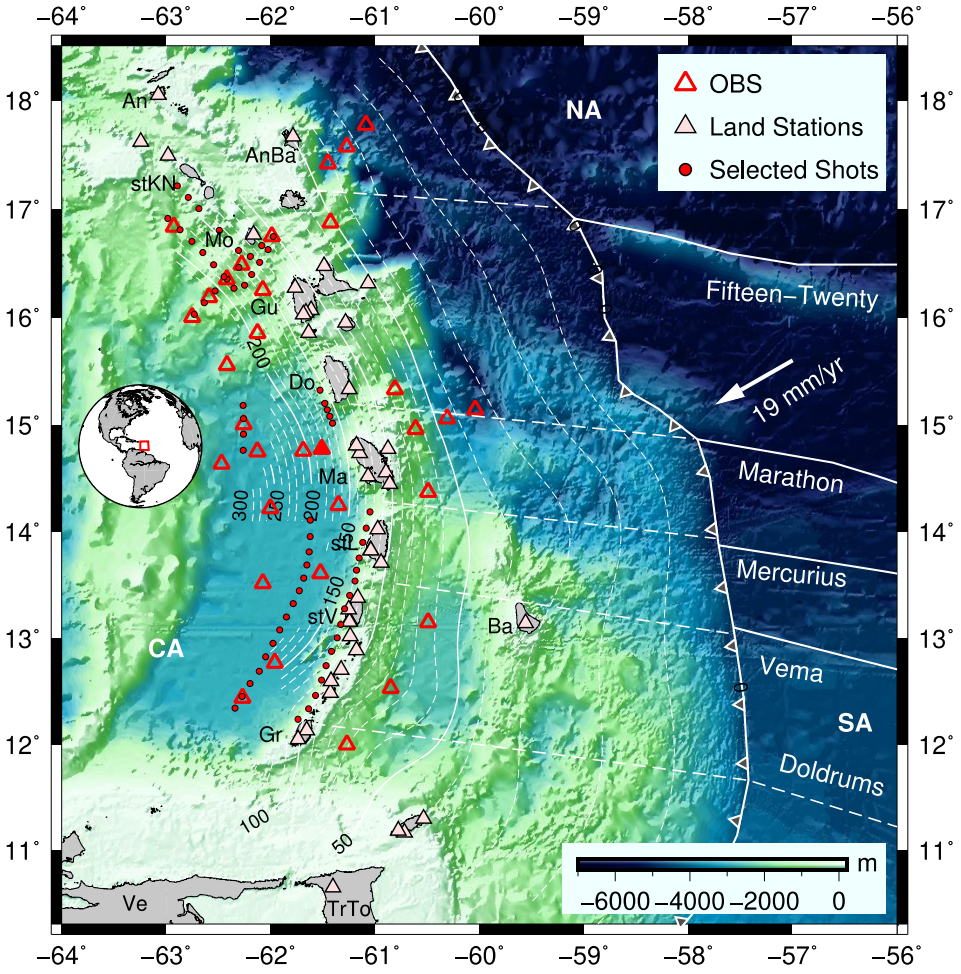

Figure 1. Tectonic map of the Lesser Antilles subduction zone. Offshore and onshore seismic stations used in this study are marked by empty red and filled triangles, respectively. Light white contours depict refined slab geometry from this study. Reference station in the 1-D velocity inversion is filled by red colour. Red dots in the back-arc indicate active shots included in the inversion. Details of land stations incorporated in this study are shown in Figure S1. Inferred fracture zone and spreading-ridge structures (Schlaphorst *et al.,* 2016) are shown with white lines. CA: Caribbean Plate; NA: North American Plate; SA: South American Plate. See Figure S1 for details of island name abbreviations.

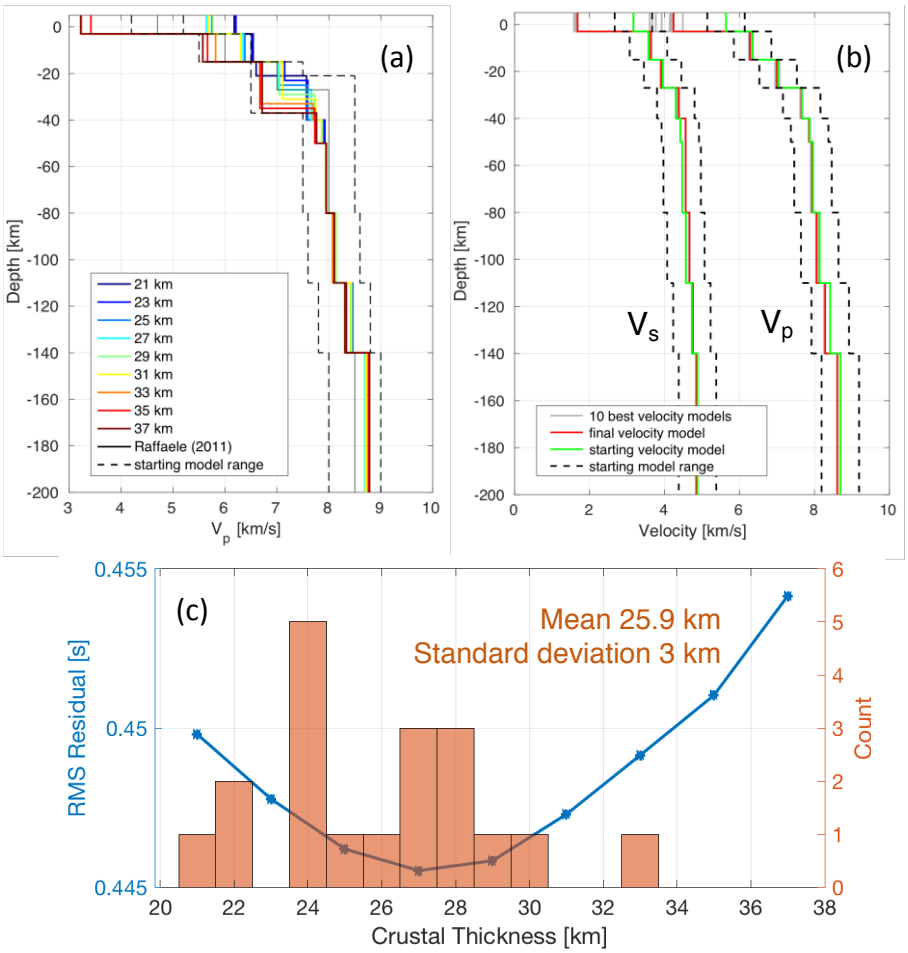

Figure 2. (a) Best v_p models for simulations with different starting velocity layer configuration. The crustal thickness is varied from 21 km to 37 km, in 2 km increments. (b) Final v_p and v_s models for the Lesser Antilles subduction zone. (c) RMS residual versus the tested crustal thickness. The minimum RMS misfit is achieved with a crustal thickness of 27 km. The bar chart shows the distribution of crustal thickness derived by González et al. (2018) from 19 land stations along the arc.

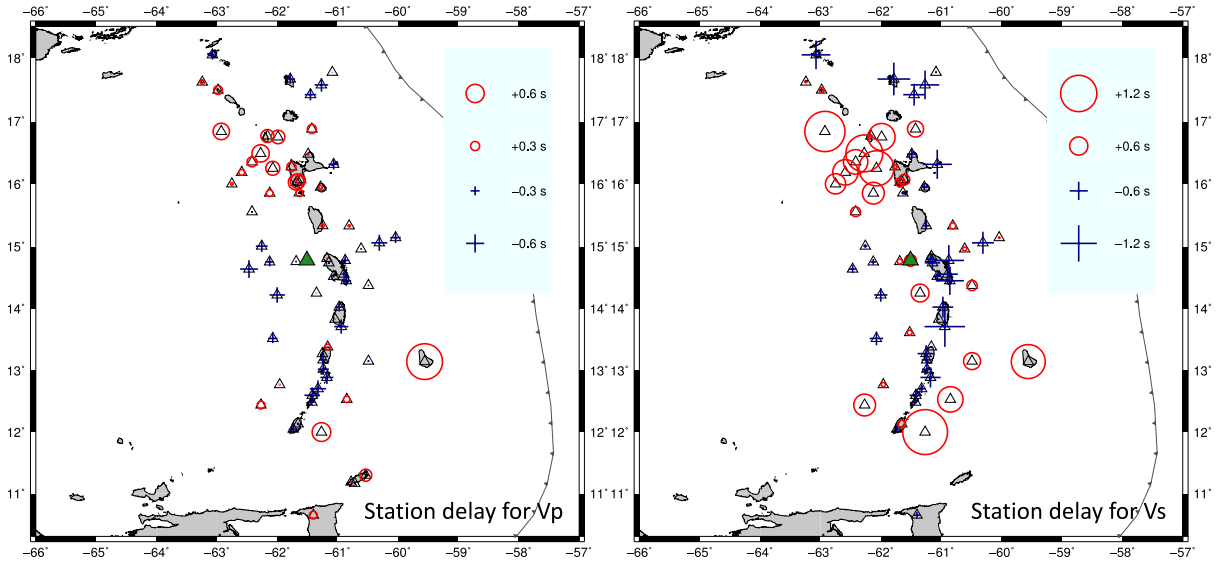

734

735 Figure 3. Station corrections associated with the velocity model shown in Figure 2b.

736

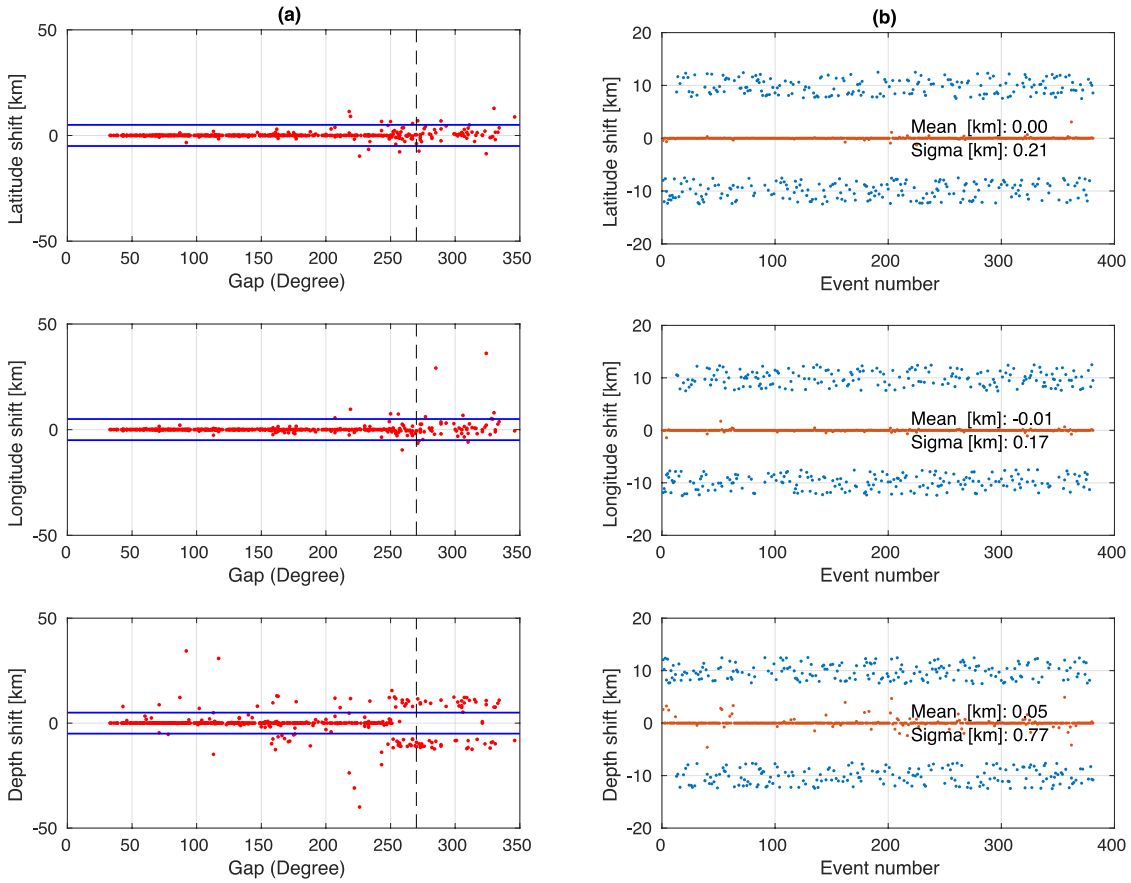

Figure 4. Stability test using the velocity model shown in Figure 2b to recover the randomly perturbed earthquakes (blue points) in the longitude, latitude and depth directions. Those recovered (red points) to be within 5 km (marked as blue line in the left panels) from their original locations and having azimuthal gap smaller than 270° (black dashed line) are deemed as events with good quality and shown in Figure 5 and 6. The panels on the right side show the mean and standard deviation of the difference between the recovered (red points) and perturbed (blue points) earthquake locations in three directions for good quality events.

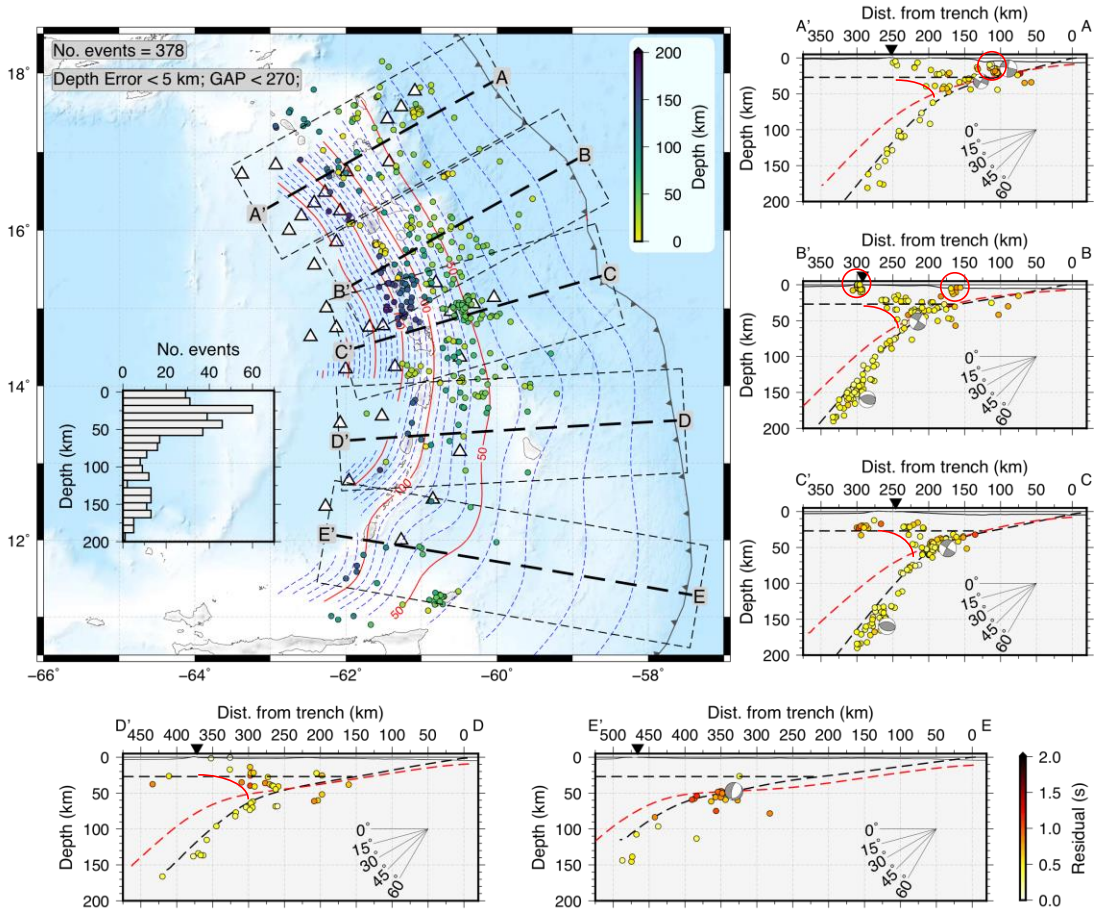

Figure 5. Distribution of the relocated 378 events coloured by hypocentral depth. The inset shows the number of events versus depth. Triangles are the stations from the VoiLA OBS deployment. Dashed blue and red lines represent the refined slab geometry from this study. Red curve delineates the wedge-shaped mantle corner seismicity. Depth profiles through the regional events comprise earthquakes that are within 75 km perpendicular distance of the labelled lines on the map. In the profiles, earthquakes are coloured by their RMS misfit after the relocation using the best 1-D velocity models from this study. The side hemisphere focal mechanisms from the Global Centroid Moment Tensor Project (see Data and Resources) are plotted. Black dashed curves are from slab model generated in this study, while the red dashed curves are from Slab2.0 (Hayes et al., 2018).

760

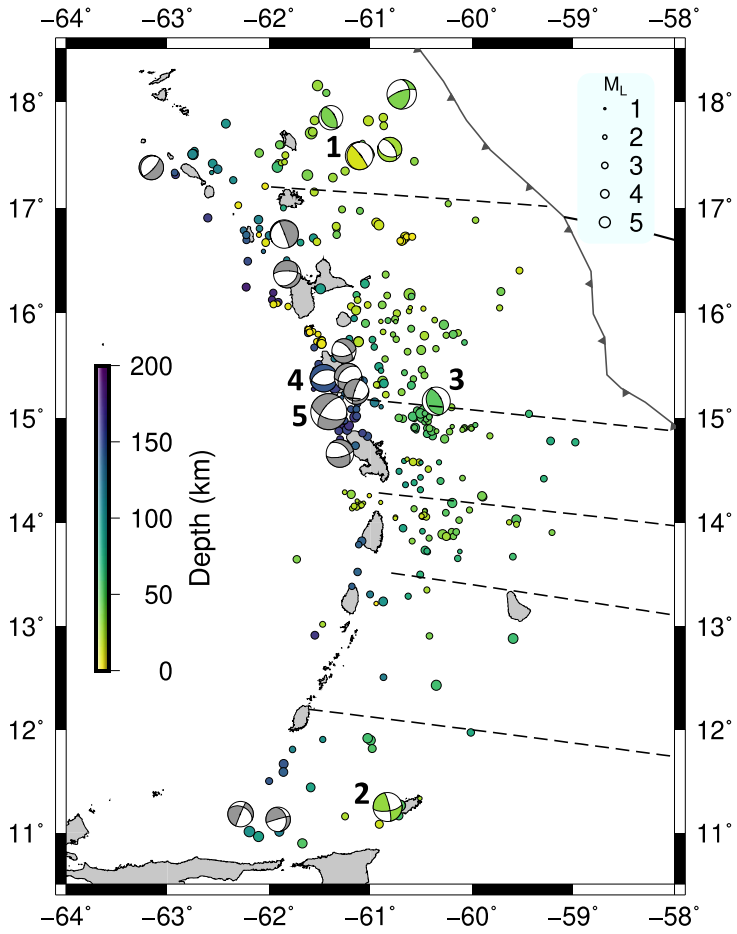

761

762 Figure 6. Local seismicity as derived from this study. Focal mechanisms (FM) for events
763 with GCMT (see Data and Resources) solutions during the period of passive-seismic
764 experiments are coloured by depth. Focal mechanisms for all historical deep (> 70 km)
765 normal fault events (at least one slip direction between -145° and -90°) in the GCMT
766 catalogue and from Gonzalez et al. (2017) are marked in grey. FM 1: M_w 5.7,
767 2017/04/17; FM 2: M_w 5.9, 2016/12/06; FM 3: M_w 5.8, 2017/02/03; FM 4: M_w 5.6,
768 2016/10/18; FM 5: M_w 7.4, 2007/11/29.

769

Figure

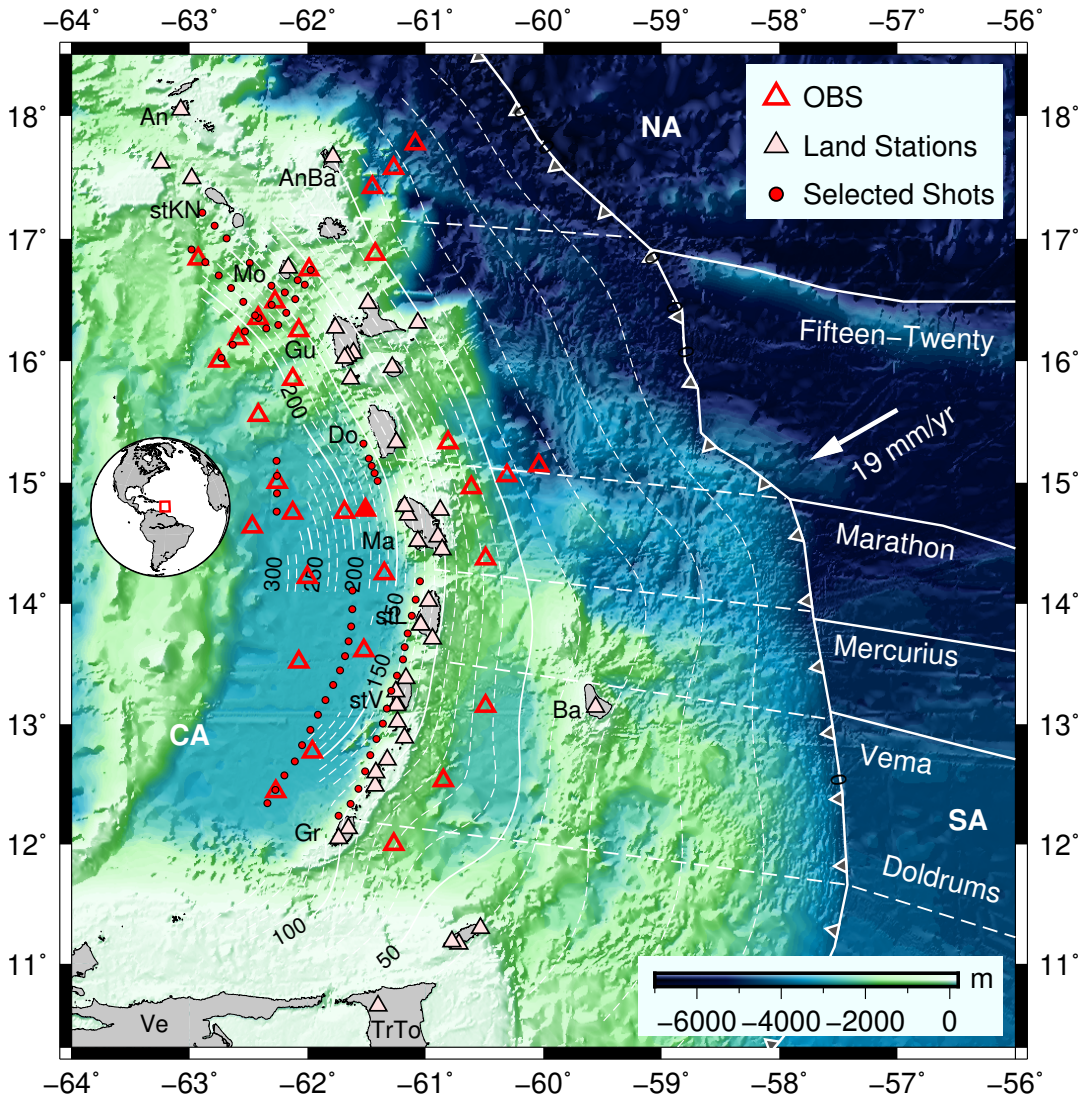
OBS
Land Stations
Selected Shots
NA
CA
SA
Fifteen–Twenty
19 mm/yr
Marathon
Mercurius
Vema
Doldrums
An
AnBa
stKN
Mo
Gu
Do
Ma
stL
stV
Gr
Ba
Ve
TrTo
100
200
300
250
200
150
100
50
50
m
−6000 −4000 −2000 0
−64˚ −63˚ −62˚ −61˚ −60˚ −59˚ −58˚ −57˚ −56˚
18˚ 17˚ 16˚ 15˚ 14˚ 13˚ 12˚ 11˚

Figure

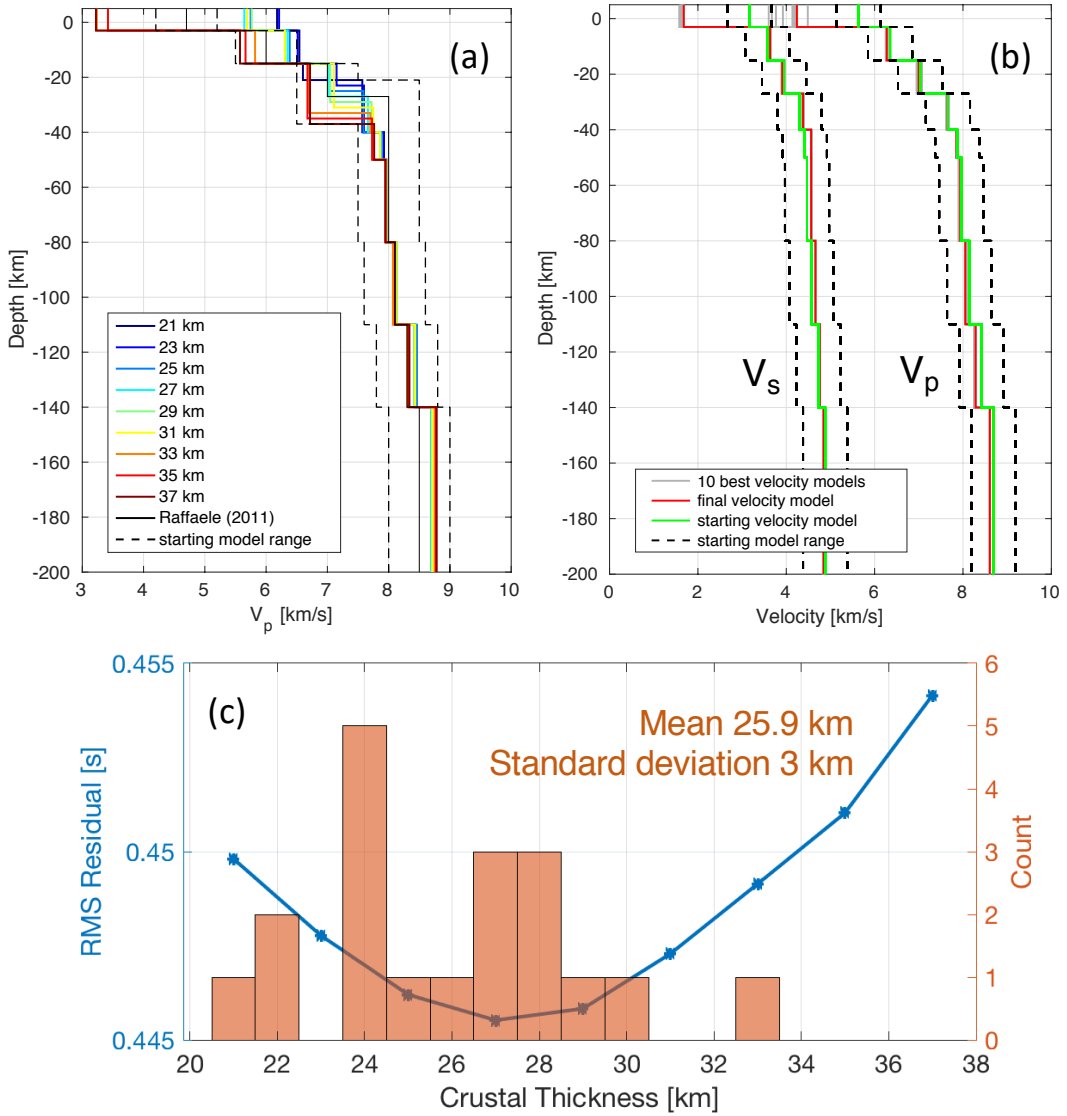
(a)
Depth [km]
V_p [km/s]
21 km
23 km
25 km
27 km
29 km
31 km
33 km
35 km
37 km
Raffaele (2011)
starting model range
(b)
V_s
V_p
Velocity [km/s]
10 best velocity models
final velocity model
starting velocity model
starting model range
(c)
Mean 25.9 km
Standard deviation 3 km
RMS Residual [s]
Count
Crustal Thickness [km]

Figure

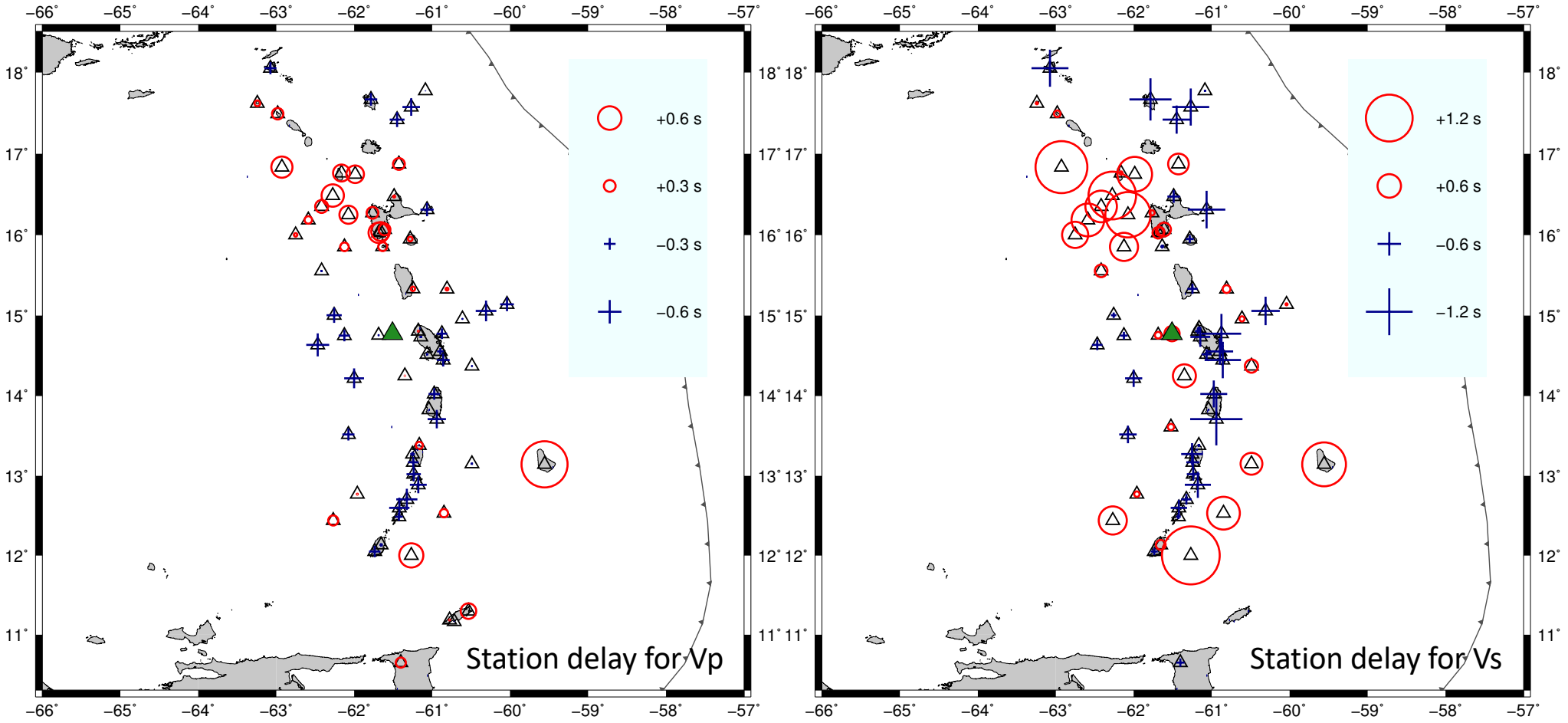
+0.6 s
+0.3 s
−0.3 s
−0.6 s
Station delay for Vp
+1.2 s
+0.6 s
−0.6 s
−1.2 s
Station delay for Vs

Figure

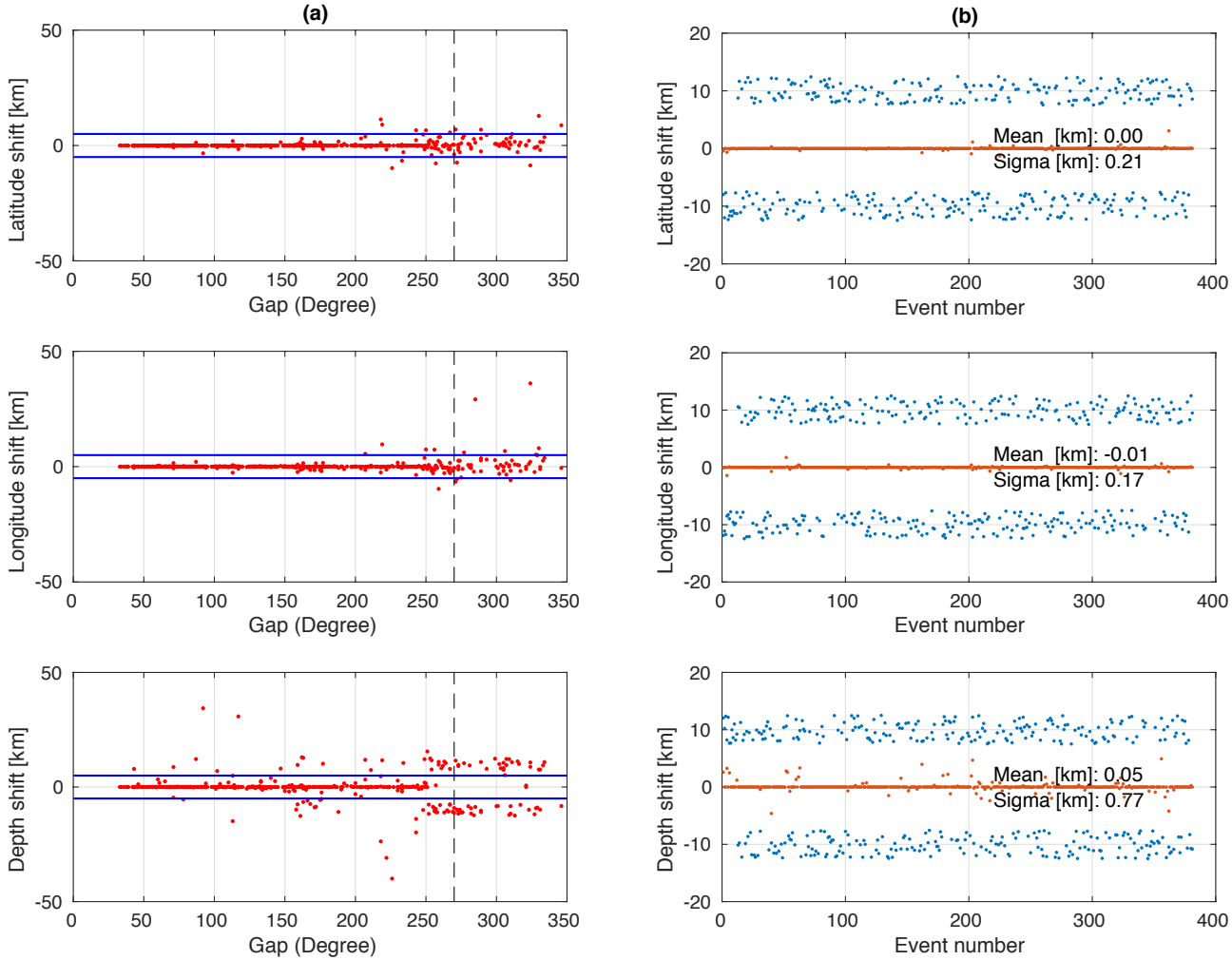
(a)
(b)
Latitude shift [km]
Longitude shift [km]
Depth shift [km]
Gap (Degree)
Event number
Mean [km]: 0.00
Sigma [km]: 0.21
Mean [km]: -0.01
Sigma [km]: 0.17
Mean [km]: 0.05
Sigma [km]: 0.77

Figure

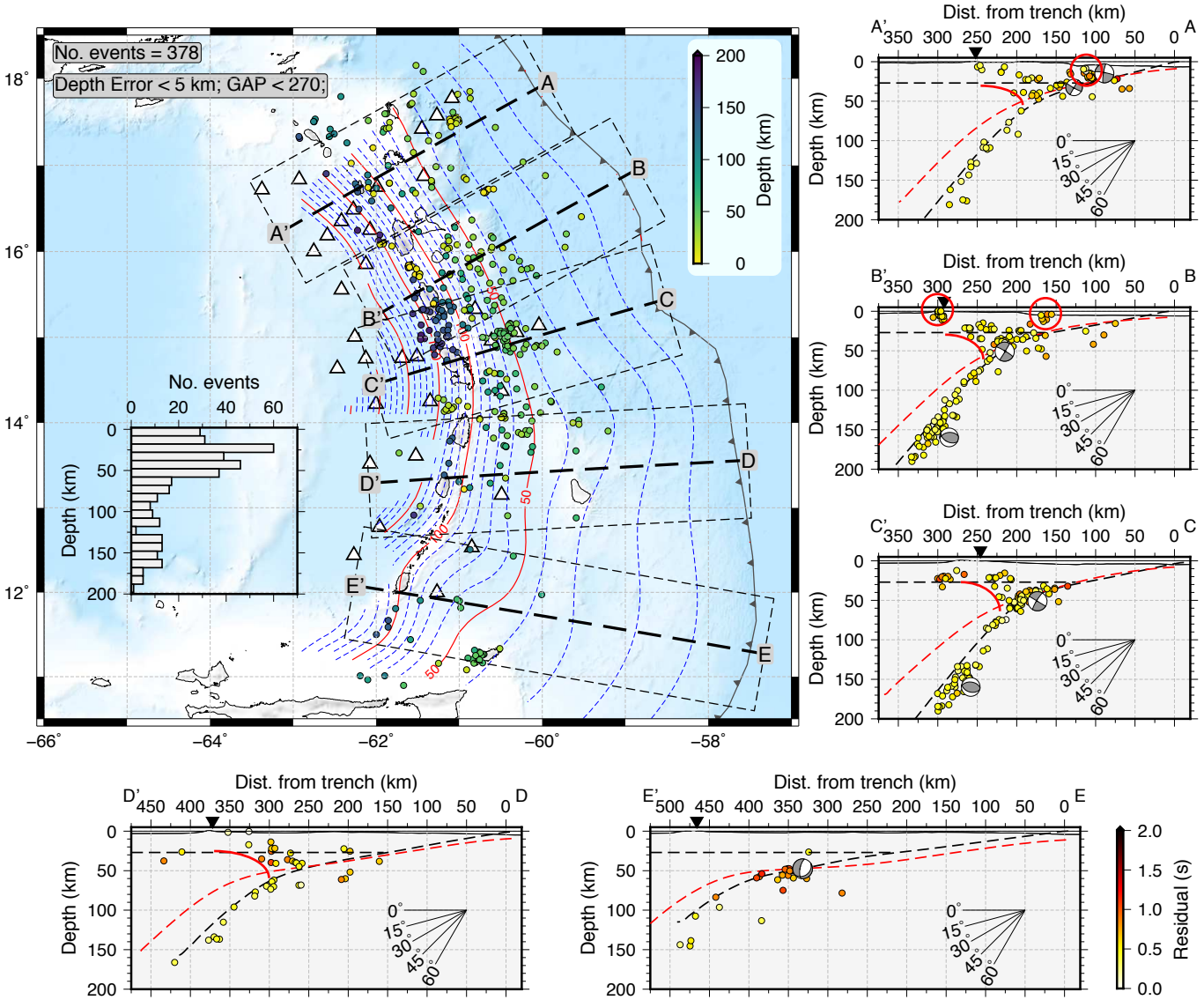
No. events = 378
Depth Error < 5 km; GAP < 270;
Depth (km)
No. events
Dist. from trench (km)
A'
A
B'
B
C'
C
D'
D
E'
E
0°
15°
30°
45°
60°
Residual (s)
18°
16°
14°
12°
−66°
−64°
−62°
−60°
−58°

Figure

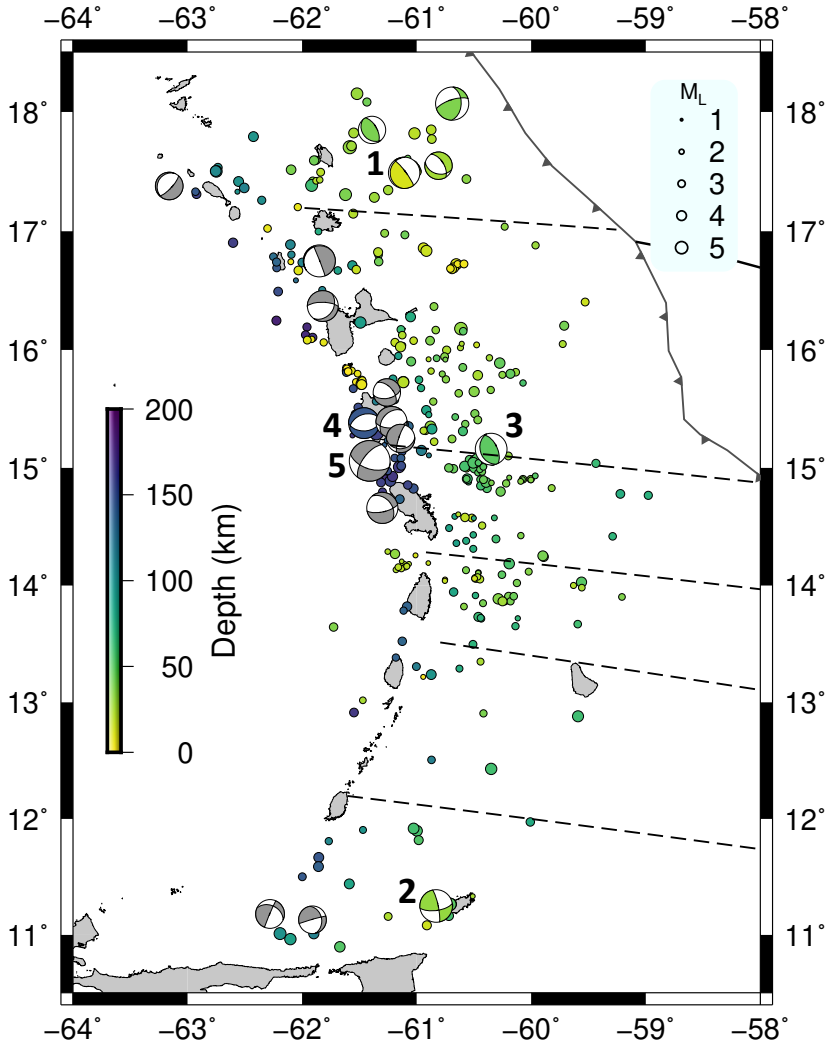
−64˚
−63˚
−62˚
−61˚
−60˚
−59˚
−58˚
18˚
17˚
16˚
15˚
14˚
13˚
12˚
11˚
M_L
1
2
3
4
5
Depth (km)
200
150
100
50
0
1
2
3
4
5

Supplementary data for

Along arc heterogeneity in local seismicity across the Lesser Antilles subduction zone from a dense ocean-bottom seismometer network

Lidong Bie, Andreas Rietbrock, Stephen Hicks, Robert Allen, Jon Blundy, Valerie Clouard, Jenny Collier, Jon Davidson, Thomas Garth, Saskia Goes, Nick Harmon, Tim Henstock, Jeroen van Hunen, Mike Kendall, Frank Krüger, Lloyd Lynch, Colin Macpherson, Richard Robertson, Kate Rychert, Stephen Tait, Jamie Wilkinson, Marjorie Wilson

Corresponding author: Lidong Bie (l.bie@liv.ac.uk)
Geophysical Institute, Karlsruhe Institute of Technology, Germany
*Also at Department of Earth Ocean & Ecological Sciences, University of Liverpool, UK

Figure S1 adds details of the local network and island names. Figures S2 and S3 show the quality of magnitude estimation. Figure S4 shows the relationship between station correction and elevation. Figure S5 shows the comparison of our slab geometry with that of Slab2.0. Figure S6 shows seismicity projected to dense profiles in the central part of the arc. Table S1 describes the optimal 1-D velocity model. Table S2 shows 378 well-relocated events.

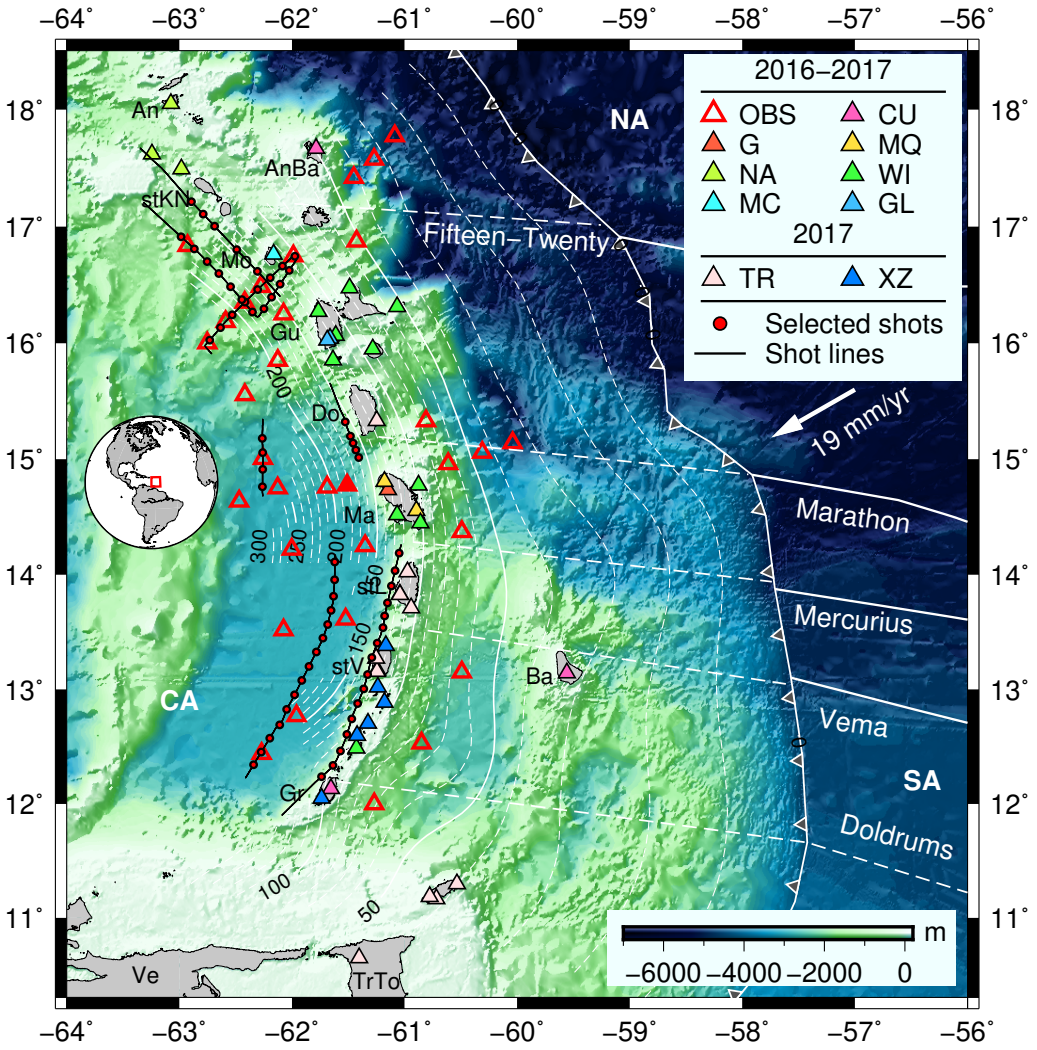

Figure S1. Similar to Figure 1. Black lines show active shots in the back-arc. This study includes seismic data from permanent stations of the following networks: the USGS Caribbean Network (code: CU); the Eastern Caribbean Seismic Network of UWI-SRC (code: TR); the West Indies French Seismic Network (code: WI); the Guadeloupe Volcano and Seismic Observatory network (code: GL); the Martinique Volcano Observatory (code: MQ); the GEOSCOPE network (code: G); the Montserrat CALIPSO Borehole Network (code: MC); and the Netherlands Antilles Seismic Network (code: NA). Our temporal network of land stations installed in 2017 is assigned code XZ. An: Anguilla; AnBa: Antigua & Barbuda; stKN: st. Kitts & Nevis; Mo: Montserrat; Gu: Guadeloupe; Do: Dominica; Ma: Martinique; stL: st. Lucia; stV: st. Vincent; Gr: Grenada; Ba: Barbados; Ve: Venezuela; TrTo: Trinidad & Tobago.

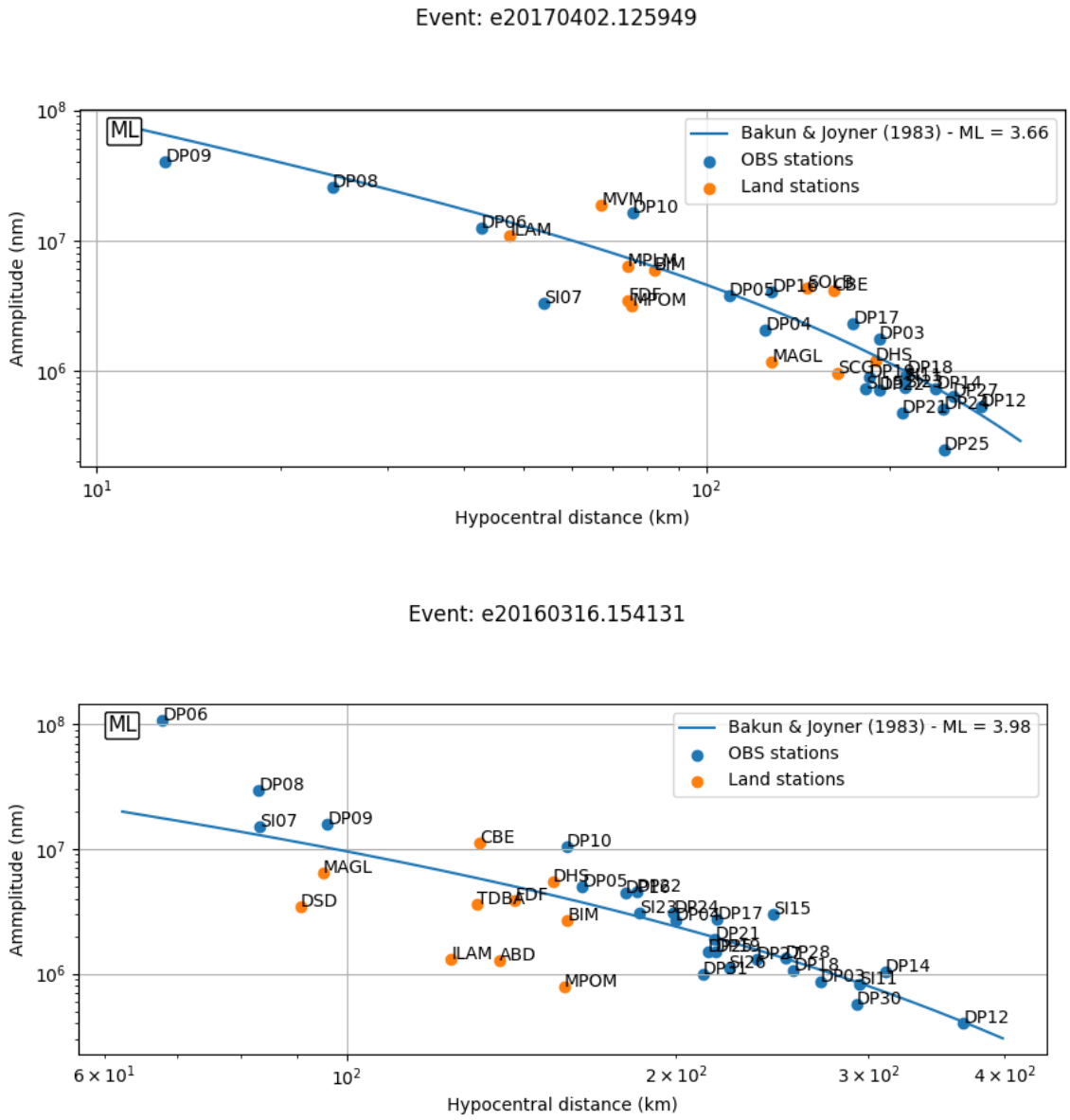

Figure S2. Example amplitude-distance plot showing the M_L fit. Overall, the M_L scale fitting robustly both the OBS and the land stations.

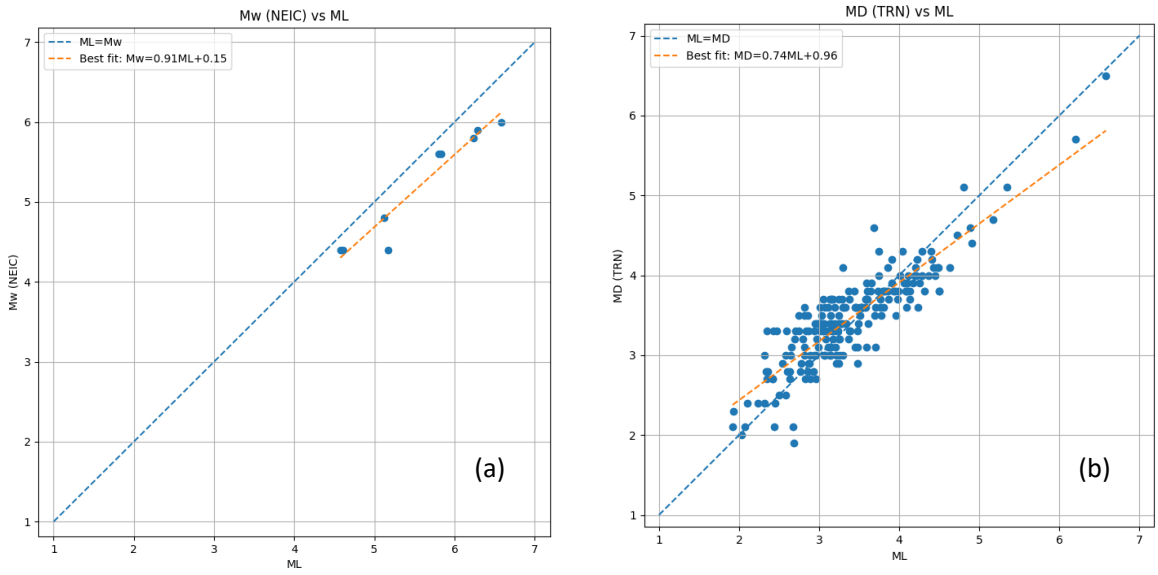

Figure S3. (a) Correlation between our M_L and moment magnitude (M_w) from NEIC. (b) Correlation between our M_L and duration magnitude (M_d) from SRC.

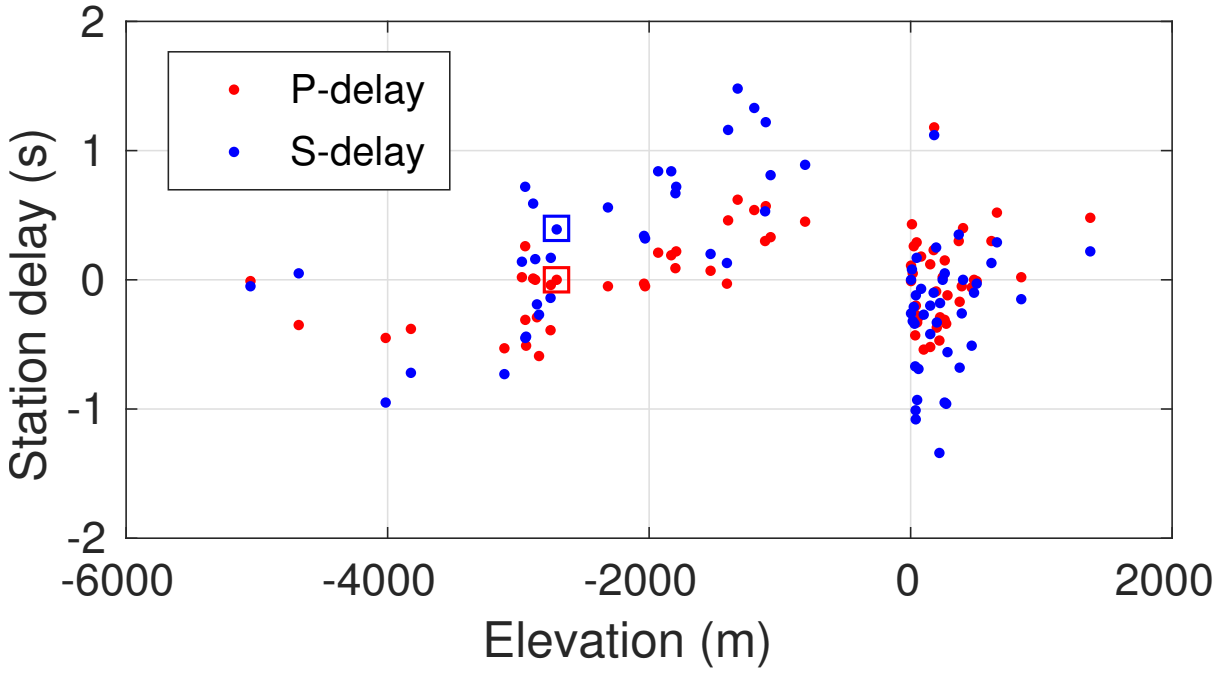

Figure S4. Station correction versus elevation. Rectangle is the reference station.

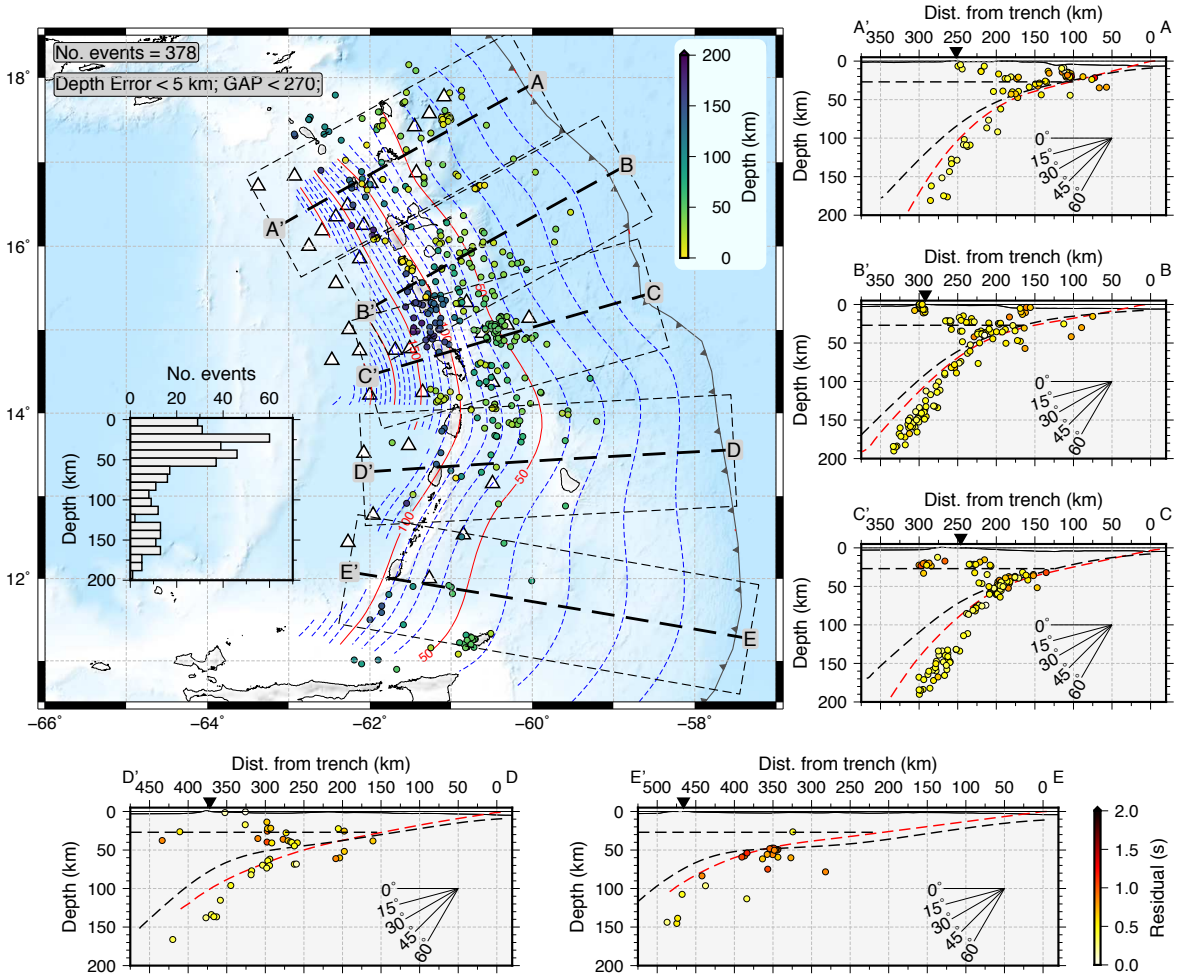

Figure S5. Similar to Figure 5, but with slab contours from Bie et al. (2017). Profiles show how slab curves fit the local seismicity reported by this study. Red dashed curves are from slab model in Bie et al. (2017), while the black dashed curves are from Slab2.0 (Hayes et al., 2018).

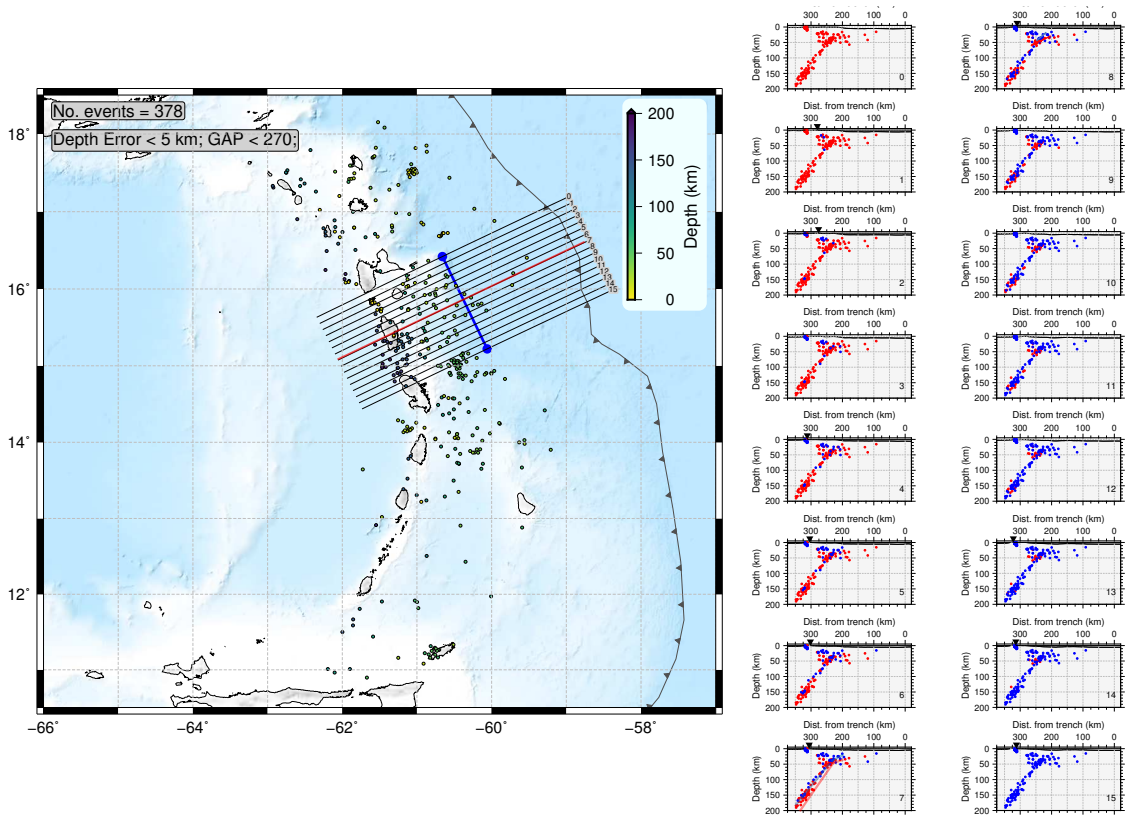

Figure S6. Seismicity bounded by line 0 and 15 are projected onto multiple profiles roughly parallel to the subduction direction. Profiles are taken every 10 km with seismicity to the north of the profile marked in blue, and those to the south in red. Profile 7 indicates increased Wadati-Benioff zone thickness from north (blue line) to south (red line), and no obvious slab tear was observed.

Table S1. Minimum 1D velocity model derived in this study by inverting 265 events with GAP≤180° and more than 20 P- and 5 S-arrival picks.

Depth (km)	V_p (km/s)	V_s (km/s)
-5	4.24	1.68
3	6.28	3.63
15	7.00	3.91
27	7.65	4.38
40	7.85	4.56
50	7.94	4.56
80	8.05	4.66
110	8.29	4.76
140	8.61	4.85
200	9.14	5.35

Table S2. Locations of the final 378 events.

Date	Time	Latitude	Longitude	Depth (km)	M_L	RMS (s)
16-03-09	10:53:08.66	11.1595	-61.2497	24.44	3.21	0.44
16-03-09	23:33:45.26	14.5876	-60.6681	81.04	2.42	0.32
16-03-14	04:19:12.80	15.0150	-60.4095	48.73	2.00	0.25
16-03-16	09:26:09.16	15.8203	-60.8743	22.75	2.65	0.53
16-03-16	12:52:01.71	13.9081	-60.1534	44.71	3.13	0.41
16-03-16	15:41:32.33	15.7854	-60.4672	25.77	3.97	0.27
16-03-16	16:30:49.46	11.5011	-61.9985	143.75	3.25	0.28
16-03-17	01:10:31.36	16.9697	-61.1031	43.81	3.30	0.53
16-03-17	18:31:25.85	15.0137	-60.5814	58.32	4.23	0.44
16-03-18	09:07:18.28	15.3052	-61.0999	131.68	3.59	0.39
16-03-22	14:09:36.17	17.3081	-61.6214	39.38	4.88	0.46
16-03-23	15:01:31.92	14.1830	-61.0670	23.51	2.03	0.66
16-03-25	20:42:25.15	15.8407	-61.6094	0.75	3.18	0.29
16-03-28	06:31:40.05	14.1902	-60.8984	17.17	1.93	0.93
16-03-29	06:48:21.42	17.8511	-60.8729	21.60	3.99	1.23
16-03-30	23:04:52.78	14.1431	-61.1333	19.52	2.67	0.72
16-03-31	05:20:55.27	14.4305	-60.5066	75.60	2.58	0.27
16-04-01	23:20:25.77	15.1018	-60.2002	31.70	3.23	0.42
16-04-04	07:21:45.93	14.8483	-60.4403	59.77	3.46	0.44
16-04-05	21:08:06.00	15.0835	-61.1370	141.10	3.26	0.41
16-04-07	22:12:36.68	14.0591	-60.4949	13.71	2.45	0.63
16-04-07	22:20:54.10	14.0525	-60.4479	21.80	3.16	0.69
16-04-08	03:11:03.11	15.9323	-60.3648	27.32	2.59	0.39
16-04-09	10:56:03.85	14.9664	-60.4288	44.23	2.83	0.30
16-04-10	04:21:15.35	14.6049	-60.6369	21.51	2.00	0.53
16-04-11	08:11:56.99	13.8195	-61.0837	136.73	3.87	0.36
16-04-11	09:59:37.02	16.5860	-62.0547	128.54	2.00	0.28
16-04-11	21:03:27.60	13.7315	-60.4620	64.01	3.77	0.49
16-04-12	01:44:50.42	14.9053	-60.0045	34.60	3.01	0.64
16-04-12	08:47:17.89	14.8977	-60.0034	36.09	2.35	0.72
16-04-12	12:36:33.62	15.7107	-61.4827	10.91	4.49	0.69
16-04-12	15:24:27.59	15.7064	-61.4804	6.33	4.10	0.58
16-04-13	03:08:58.16	13.3064	-61.0031	115.18	3.21	0.37
16-04-15	12:20:22.03	14.2882	-61.2530	22.40	2.32	0.78
16-04-16	23:29:28.30	15.7981	-61.5153	6.72	2.82	0.47
16-04-17	03:19:34.46	14.9328	-59.9656	51.70	2.41	0.67
16-04-18	01:01:42.30	14.5754	-60.3217	63.94	2.36	0.53
16-04-20	13:14:36.35	14.9872	-60.4486	49.05	2.63	0.37
16-04-21	16:17:56.66	16.4918	-62.2093	151.51	3.61	0.28
16-04-22	11:30:52.73	14.8728	-60.3472	39.04	2.34	0.66
16-04-22	17:43:19.33	17.7728	-60.8678	23.85	3.65	0.59
16-04-23	09:16:07.78	15.4901	-60.9159	82.11	3.80	0.61
16-04-23	12:07:05.04	15.0726	-60.5000	50.54	3.20	0.42
16-04-23	15:35:21.30	11.9047	-61.4689	96.38	2.94	0.26
16-04-24	09:09:41.86	13.0181	-61.4698	26.27	2.74	0.55
16-04-24	21:01:41.09	13.9140	-60.4874	73.44	2.58	0.33
16-04-25	05:56:16.69	15.3144	-60.9230	21.21	3.11	0.49
16-04-28	03:22:33.36	14.9064	-60.5648	50.24	2.93	0.50
16-04-28	05:40:58.22	16.0781	-60.8840	38.33	3.60	0.49
16-04-28	20:14:59.92	15.3166	-60.9393	21.45	3.00	0.48
16-05-01	10:35:35.55	18.1520	-61.5212	30.48	4.81	0.62
16-05-02	14:05:29.53	16.8880	-62.1028	109.09	3.91	0.37
16-05-02	15:09:55.79	15.8168	-61.5988	-0.19	3.17	0.42
16-05-04	21:06:32.70	14.5784	-60.5782	18.53	3.51	0.60
16-05-05	02:23:26.02	14.9758	-61.4646	184.31	3.53	0.48
16-05-06	13:15:46.40	11.8078	-61.7669	107.58	2.96	0.46
16-05-06	13:49:31.22	16.1244	-61.1265	23.20	3.14	0.58
16-05-07	05:23:25.85	17.3452	-61.2489	27.25	3.83	0.45
16-05-08	13:48:04.53	17.7046	-61.5840	32.53	5.35	0.77
16-05-09	00:21:50.57	17.6963	-61.5937	31.04	3.43	0.52
16-05-09	13:36:27.76	16.1791	-60.6147	32.34	5.17	0.51
16-05-09	15:03:38.41	16.1579	-60.5937	50.37	3.09	0.59
16-05-09	20:04:41.80	14.1632	-61.0872	19.78	2.51	0.71
16-05-10	06:21:14.02	16.7254	-60.5881	3.95	3.29	0.66
16-05-14	22:12:22.75	14.1328	-61.1803	23.33	2.44	1.04
16-05-15	08:17:07.36	14.1558	-61.1601	20.31	2.81	0.80

16-05-15	16:09:15.03	13.3840	-61.1817	137.99	2.96	0.29
16-05-17	02:08:26.10	15.0090	-60.4183	50.27	2.78	0.38
16-05-17	11:41:17.04	14.7345	-61.1478	133.88	3.59	0.32
16-05-20	01:24:47.25	14.2049	-61.1311	22.55	1.92	0.58
16-05-20	06:18:29.94	15.8104	-60.1353	30.62	3.15	0.64
16-05-21	22:17:56.58	14.1704	-61.1121	22.32	3.39	0.69
16-05-24	09:04:33.96	15.7970	-60.1822	47.83	3.74	0.56
16-05-24	17:11:07.47	16.6854	-60.7059	5.09	3.17	0.50
16-05-24	23:19:40.48	11.3335	-60.5114	26.44	2.00	0.49
16-05-26	04:40:55.73	16.8810	-59.9632	30.04	3.04	0.74
16-05-28	18:58:51.45	14.2564	-61.0099	12.23	2.08	0.35
16-05-30	02:52:58.32	14.0395	-60.7542	17.18	2.10	0.34
16-05-30	18:55:21.10	14.1857	-60.1926	57.35	4.31	0.67
16-06-02	10:04:47.26	16.0890	-61.9155	4.68	2.60	0.21
16-06-05	12:45:48.27	14.0277	-59.5608	51.78	4.17	0.67
16-06-05	13:07:55.57	13.9994	-59.6307	22.27	2.54	0.43
16-06-05	13:09:06.93	13.9808	-59.5586	25.45	2.82	0.61
16-06-09	03:38:32.47	11.8971	-60.9981	57.60	4.45	0.82
16-06-10	01:45:16.98	15.3293	-60.8674	81.89	4.09	0.50
16-06-12	08:56:55.92	16.8581	-60.9412	13.19	4.29	0.50
16-06-13	18:31:31.84	15.2783	-61.1863	145.38	4.25	0.55
16-06-18	20:08:33.36	15.4089	-61.2030	117.02	3.26	0.35
16-06-20	21:57:16.77	14.8762	-60.3946	51.33	4.10	0.37
16-06-22	00:50:28.14	13.4967	-60.5094	69.64	3.21	0.38
16-06-23	20:03:29.22	13.9437	-60.6777	82.17	3.49	0.32
16-06-25	00:27:21.28	16.7131	-61.5612	91.78	3.80	0.37
16-06-25	11:58:01.77	15.5776	-61.1914	100.40	3.25	0.31
16-06-29	14:16:09.21	16.1668	-60.8335	31.99	3.12	0.44
16-06-29	15:54:22.87	15.3685	-61.1193	132.18	4.48	0.52
16-06-30	00:58:55.86	14.8546	-61.0775	158.01	3.53	0.37
16-06-30	23:04:35.50	15.4570	-61.5372	150.52	3.29	0.31
16-07-01	05:41:56.88	16.0630	-61.1892	17.09	3.37	0.39
16-07-02	04:14:52.99	14.8283	-59.8211	32.10	2.89	1.06
16-07-06	11:05:56.03	15.0181	-61.1350	152.51	3.57	0.38
16-07-07	09:33:45.63	15.9205	-60.8967	22.49	2.00	0.37
16-07-11	06:58:09.58	15.7260	-61.1169	21.22	4.50	0.38
16-07-11	06:58:09.61	15.7287	-61.1176	23.81	4.50	0.49
16-07-13	10:28:25.05	15.2462	-60.6919	34.69	3.24	0.34
16-07-14	18:09:40.04	15.3155	-61.2106	132.61	3.48	0.44
16-07-18	11:15:20.63	15.6725	-61.5541	149.86	3.27	0.34
16-07-19	18:57:40.51	15.6479	-60.4986	36.06	4.20	0.50
16-07-25	04:59:44.09	15.5637	-61.3561	112.29	3.05	0.29
16-07-25	15:57:08.87	16.6772	-61.5268	16.77	3.51	0.52
16-07-25	19:30:43.22	16.6696	-62.0322	10.28	3.58	0.37
16-07-26	03:27:22.06	16.6701	-61.6885	86.68	3.09	0.30
16-07-26	17:50:04.38	15.9487	-61.1604	88.96	3.05	0.54
16-07-29	13:55:02.01	15.7893	-60.2517	34.18	2.88	0.45
16-08-01	03:43:03.21	14.8774	-61.3117	160.14	3.58	0.48
16-08-02	00:13:09.34	15.1445	-61.4591	171.05	3.48	0.42
16-08-02	07:58:32.85	15.1543	-60.3870	46.81	4.63	0.51
16-08-04	23:26:26.99	14.9932	-60.6788	46.38	3.45	0.30
16-08-05	16:21:15.16	14.9002	-60.4179	45.12	3.19	0.44
16-08-07	13:10:23.27	15.1378	-60.4086	43.32	3.01	0.40
16-08-08	10:15:56.26	17.3848	-61.9171	62.15	4.91	0.48
16-08-09	03:53:15.58	15.5623	-60.8552	34.70	3.04	0.49
16-08-10	05:07:31.13	14.9592	-60.4659	49.94	2.64	0.45
16-08-10	19:20:33.43	15.7398	-61.1132	21.62	3.08	0.33
16-08-11	21:21:39.52	13.7187	-60.1178	68.21	2.20	0.13
16-08-13	02:22:35.53	17.0238	-62.3014	6.58	3.13	0.41
16-08-15	12:36:29.60	14.9719	-61.2589	155.41	3.30	0.45
16-08-15	19:06:27.25	14.9041	-60.0723	37.50	3.15	0.59
16-08-16	05:24:15.88	17.4239	-61.8781	22.62	2.71	0.53
16-08-16	10:57:42.64	11.5887	-61.8569	138.63	4.10	0.52
16-08-17	13:38:31.34	15.3731	-60.5758	42.04	2.97	0.82
16-08-18	22:51:39.07	15.5133	-61.5110	154.15	3.46	0.36
16-08-19	07:21:38.12	16.0263	-61.1417	20.60	4.22	0.54
16-08-20	02:16:33.57	11.8165	-60.9822	53.92	3.69	1.10
16-08-23	01:09:49.90	14.8897	-61.2307	156.59	4.41	0.37
16-08-23	16:58:20.84	15.4605	-60.4928	40.64	3.37	0.53
16-08-23	17:10:05.90	17.2027	-62.0384	6.65	2.98	0.41

16-08-23	19:25:26.72	15.7416	-61.4788	5.95	2.76	0.37
16-08-24	17:03:03.05	14.2683	-61.1897	32.98	3.80	0.64
16-08-26	00:49:42.76	14.9743	-61.2531	150.35	3.11	0.52
16-08-26	22:20:24.69	14.9018	-60.4426	51.87	3.07	0.78
16-08-27	22:12:25.61	15.1388	-61.1272	148.89	3.25	0.49
16-08-27	22:40:56.70	13.2883	-60.6266	76.97	2.86	0.42
16-08-31	02:30:44.05	15.2753	-61.5602	167.89	2.00	0.43
16-09-05	07:15:36.57	14.8279	-60.3866	55.45	3.58	0.49
16-09-05	12:12:19.98	17.2845	-61.3701	29.76	4.06	0.57
16-09-06	05:31:48.12	14.8682	-60.2186	37.96	3.01	0.78
16-09-07	02:42:21.53	16.2046	-59.7119	41.76	3.75	0.72
16-09-07	03:38:01.15	15.7196	-60.0715	57.02	2.69	0.79
16-09-08	11:45:47.93	13.8654	-60.2280	37.92	3.06	0.66
16-09-08	18:53:03.95	15.0258	-61.4593	184.95	3.21	0.51
16-09-08	21:39:51.28	15.0812	-61.3608	182.18	4.11	0.46
16-09-10	05:34:48.29	15.2228	-60.8473	21.30	3.14	0.55
16-09-11	23:16:03.27	16.0396	-61.1192	14.90	2.32	0.55
16-09-13	09:34:25.61	12.9053	-60.4175	39.72	3.06	1.02
16-09-18	01:08:40.64	16.0634	-61.8121	7.87	3.01	0.65
16-09-19	00:48:51.56	15.9978	-60.7382	24.09	3.37	0.55
16-09-19	08:42:27.68	15.9425	-60.7565	36.50	3.29	0.50
16-09-19	14:33:31.06	14.9847	-61.4180	183.69	4.72	0.45
16-09-23	01:48:34.40	17.7937	-62.4255	96.05	4.04	0.56
16-09-24	05:42:03.61	14.0905	-60.2558	50.23	3.15	0.68
16-09-25	11:20:01.75	14.3112	-60.5063	74.35	2.94	0.36
16-09-25	23:09:27.13	15.3838	-61.3099	0.30	2.47	0.58
16-09-26	02:16:32.07	14.9955	-60.5664	23.76	2.95	0.46
16-09-26	15:41:24.55	14.4182	-59.2894	68.85	3.15	0.74
16-09-26	20:36:18.73	15.3945	-61.3102	-0.18	2.42	0.56
16-09-30	18:57:04.07	13.9059	-60.1981	39.49	3.34	0.44
16-10-01	11:11:03.91	13.8641	-60.2507	27.74	3.73	0.55
16-10-02	14:53:41.24	15.7408	-61.4756	9.80	3.14	0.51
16-10-03	15:18:58.80	15.3517	-60.8800	32.29	4.47	0.51
16-10-04	03:55:40.76	15.8086	-61.6137	147.93	3.21	0.35
16-10-05	02:04:27.16	15.3106	-60.5963	60.61	3.69	0.53
16-10-05	04:21:19.98	16.0827	-61.9554	8.93	3.22	0.44
16-10-06	12:00:50.95	13.6438	-61.7255	37.72	3.51	0.88
16-10-07	06:50:21.72	12.9124	-61.5476	166.13	3.61	0.33
16-10-07	19:04:44.32	17.4953	-61.8388	20.54	3.26	0.39
16-10-09	23:03:37.25	15.9015	-61.0491	48.38	3.75	0.47
16-10-13	10:38:03.75	17.5344	-62.7350	98.38	3.46	0.28
16-10-14	17:06:46.17	16.2464	-62.2245	180.97	3.68	0.50
16-10-14	17:25:24.00	16.7226	-60.6546	10.65	4.60	0.74
16-10-15	02:26:51.65	16.7235	-60.6433	3.81	2.94	0.88
16-10-16	12:05:39.27	17.2597	-62.3534	101.81	3.35	0.36
16-10-17	15:32:00.19	16.9834	-61.2799	33.68	3.21	0.49
16-10-18	00:42:51.29	13.7843	-61.1145	136.45	3.01	0.41
16-10-18	22:08:13.75	15.2983	-61.3521	159.62	5.83	0.38
16-10-19	03:26:32.20	15.7502	-60.7451	36.28	3.00	0.40
16-10-19	19:38:32.40	15.3274	-61.4344	158.33	3.37	0.55
16-10-19	20:22:19.40	15.3136	-61.3983	158.66	3.91	0.36
16-10-20	00:58:21.86	14.3961	-60.3085	60.25	3.19	0.35
16-10-24	14:14:05.22	16.6809	-60.6911	9.66	3.68	0.68
16-10-25	18:45:34.45	16.2307	-61.4916	89.26	4.73	0.43
16-10-26	03:11:02.62	13.7161	-60.4368	61.88	2.91	0.46
16-10-26	03:20:57.64	16.4041	-59.5292	15.55	3.27	0.64
16-10-26	17:50:38.94	17.8200	-61.0188	20.27	4.66	0.67
16-10-27	19:07:52.43	11.9732	-60.0082	78.34	3.53	0.85
16-10-29	05:35:30.90	15.9287	-60.8268	49.91	2.78	0.50
16-10-29	08:21:41.40	16.6912	-62.2224	143.41	3.27	0.38
16-10-29	10:38:20.32	16.0418	-60.4774	16.31	2.39	0.81
16-10-31	11:44:35.98	16.3659	-60.8487	35.48	3.28	0.58
16-10-31	13:37:07.75	15.2325	-61.2537	133.84	2.77	0.29
16-10-31	15:04:30.48	14.1168	-60.0227	36.65	2.88	0.70
16-11-02	03:29:29.19	13.8484	-60.4213	40.82	2.93	0.52
16-11-02	20:01:57.59	16.7402	-62.2235	133.20	3.36	0.40
16-11-03	15:01:21.21	15.4149	-61.1293	105.75	2.88	0.35
16-11-03	23:56:37.18	15.7968	-60.7762	38.42	2.53	0.45
16-11-08	17:05:00.79	15.1485	-60.9587	113.99	4.19	0.46
16-11-09	15:34:05.71	13.2374	-60.8738	96.06	4.10	0.48

16-11-10	02:29:23.26	13.3488	-60.4430	25.59	2.89	0.92
16-11-12	18:44:11.58	15.4076	-60.4669	37.33	3.25	0.65
16-11-13	05:19:02.80	15.0530	-60.3382	38.88	3.10	0.76
16-11-16	02:59:18.77	15.3288	-61.2435	139.78	3.08	0.41
16-11-16	08:41:51.77	15.3202	-61.4527	159.90	3.14	0.37
16-11-17	09:53:58.83	15.0075	-61.1537	165.62	4.64	0.43
16-11-18	07:32:33.84	16.8030	-62.0933	108.59	3.01	0.29
16-11-19	17:04:17.22	16.9035	-62.6030	162.00	3.90	0.48
16-11-19	18:05:28.89	15.6609	-60.3532	35.64	2.95	0.41
16-11-20	00:07:22.75	14.1563	-61.1005	20.73	2.56	0.61
16-11-20	00:46:50.38	15.1066	-60.8939	111.27	2.00	0.31
16-11-20	02:10:05.18	13.2184	-60.9425	1.50	2.00	0.17
16-11-20	05:41:05.56	16.0192	-60.6176	24.61	2.52	0.38
16-11-20	05:56:07.68	15.4519	-60.8953	78.17	2.57	0.50
16-11-20	09:09:55.17	14.0489	-60.7523	0.48	2.20	0.03
16-11-20	09:17:41.94	14.1090	-60.4620	38.02	2.45	0.75
16-11-20	16:06:18.84	17.5331	-61.1166	12.00	2.89	0.09
16-11-20	16:20:36.70	17.5067	-61.1042	8.63	2.03	0.19
16-11-20	17:14:03.50	14.8806	-60.5477	58.85	2.53	0.21
16-11-20	17:47:11.96	14.1065	-60.4635	35.29	2.10	0.61
16-11-20	20:11:03.56	14.0614	-60.4747	22.11	3.28	0.68
16-11-21	08:00:19.56	12.5063	-60.8702	113.30	3.09	0.39
16-11-21	14:43:38.47	14.0605	-60.4862	22.11	3.22	0.63
16-11-21	22:45:37.35	15.1037	-60.3805	52.43	2.70	0.85
16-11-22	00:02:02.37	11.9163	-61.0275	59.23	4.39	1.00
16-11-22	02:24:12.68	14.1298	-60.5703	39.34	2.92	0.55
16-11-22	04:12:25.36	12.8802	-59.5917	61.18	4.52	0.81
16-11-22	08:36:26.43	15.9181	-60.7503	39.94	2.00	0.06
16-11-22	18:37:20.68	16.9980	-61.8571	76.66	2.76	0.20
16-11-22	20:02:59.77	14.9026	-60.0743	41.78	2.21	0.52
16-11-23	06:09:38.09	14.9178	-60.1926	39.22	2.00	0.25
16-11-23	07:52:08.42	15.4317	-60.6632	52.42	2.76	0.28
16-11-23	09:58:21.74	17.6125	-61.0771	44.36	2.49	0.36
16-11-23	11:37:38.22	15.1939	-61.2828	139.14	2.00	0.28
16-11-23	12:03:19.06	13.7226	-60.4409	70.22	2.84	0.46
16-11-23	14:26:34.91	15.4324	-61.2860	124.76	3.85	0.43
16-11-23	16:40:14.20	16.7428	-62.0993	4.67	2.35	0.34
16-11-24	01:06:03.70	14.3597	-60.6537	86.38	2.72	0.24
16-11-24	02:38:10.73	14.0719	-60.4679	22.33	2.58	0.76
16-11-24	05:00:36.03	17.3318	-62.5647	97.52	2.00	0.40
16-11-24	13:48:21.59	14.5725	-60.5006	74.44	2.00	0.06
16-11-24	16:08:47.15	17.4455	-61.0970	9.50	2.00	0.33
16-11-24	21:22:03.69	16.0512	-60.6067	24.45	2.00	0.50
16-11-25	03:40:29.87	14.5102	-60.4290	22.46	3.03	0.57
16-11-25	07:28:49.65	14.4237	-60.0913	38.13	2.60	0.35
16-11-25	08:40:24.61	13.8190	-60.5875	35.12	2.82	0.89
16-11-25	14:39:18.55	15.0430	-60.4622	53.62	2.69	0.33
16-11-25	16:05:37.01	17.4306	-61.8456	22.85	2.58	0.34
16-11-25	16:41:49.56	14.8854	-60.0920	35.49	2.45	0.50
16-11-25	17:20:49.22	16.0497	-59.7258	25.18	2.84	0.48
16-11-26	08:07:50.43	17.7161	-61.5695	28.59	3.94	0.59
16-11-26	19:50:13.31	15.8878	-60.2756	46.84	4.27	0.55
16-11-27	23:28:17.28	16.5054	-61.8241	109.01	2.93	0.45
16-11-28	10:01:29.22	13.9013	-59.2085	38.21	2.77	0.64
16-11-30	18:17:31.60	16.0781	-61.0269	18.30	3.18	0.57
16-12-02	22:11:59.64	15.0058	-60.4910	52.72	4.71	0.37
16-12-05	23:55:59.38	16.6917	-60.6777	13.00	4.07	0.64
16-12-06	23:20:44.60	11.2807	-60.7710	47.61	4.32	0.94
16-12-06	23:48:53.94	11.2652	-60.7020	49.27	4.68	1.02
16-12-07	00:50:36.65	11.0823	-60.9113	15.27	3.71	1.16
16-12-07	02:37:48.63	11.1602	-60.8228	44.81	3.50	0.74
16-12-07	02:43:11.68	11.2001	-60.7562	50.28	3.87	0.88
16-12-07	03:38:12.94	11.2922	-60.7604	56.03	4.68	0.82
16-12-07	04:24:59.10	11.2632	-60.7122	50.17	5.24	0.87
16-12-07	07:54:43.72	17.0378	-60.2318	33.87	2.92	0.78
16-12-09	17:34:48.55	11.2045	-60.8426	55.69	4.50	0.72
16-12-10	11:33:15.47	13.8639	-60.1814	40.29	2.98	0.43
16-12-11	14:27:41.76	11.2212	-60.8960	61.51	4.06	0.65
16-12-13	01:24:10.85	14.7985	-60.2680	43.71	3.81	0.54
16-12-13	04:17:37.07	11.3140	-60.8163	74.92	4.81	1.07

16-12-15	22:47:12.05	16.7441	-61.3313	42.61	3.49	0.62
16-12-16	19:51:56.91	14.9272	-61.2113	167.57	4.17	0.65
16-12-21	07:16:58.94	15.0003	-60.7191	45.52	3.44	0.48
16-12-24	12:53:59.72	14.5745	-60.5188	15.53	3.22	0.69
16-12-26	22:13:45.62	11.4405	-61.5883	83.55	4.08	0.85
16-12-30	06:10:52.97	14.3791	-60.5684	77.14	2.92	0.33
17-01-01	07:22:21.71	15.2427	-61.1844	136.94	3.81	0.38
17-01-04	12:55:57.39	15.7472	-60.9799	74.13	3.17	0.41
17-01-06	15:01:38.44	11.0102	-61.8976	112.05	4.23	0.61
17-01-08	04:43:21.69	13.8851	-60.2872	36.10	4.31	0.84
17-01-08	09:51:38.90	10.9632	-62.1024	86.86	4.65	0.82
17-01-08	18:01:42.57	10.8968	-61.6706	53.03	4.31	0.92
17-01-13	16:34:17.88	14.2429	-59.8916	37.13	3.79	0.57
17-01-15	19:19:08.11	15.7291	-61.5311	3.20	2.80	0.48
17-01-17	01:33:11.91	14.2523	-59.8987	40.68	4.05	0.71
17-01-20	13:57:05.22	15.3286	-61.2474	148.03	3.26	0.45
17-01-24	19:26:18.87	16.7864	-62.2514	127.40	3.15	0.35
17-02-03	05:00:24.47	11.1646	-60.7194	59.27	3.85	0.60
17-02-03	12:08:37.99	17.4169	-62.5552	98.41	4.05	0.51
17-02-03	19:54:22.86	15.0646	-60.4572	51.14	6.23	0.41
17-02-04	13:53:08.38	14.4891	-60.7169	85.16	2.84	0.36
17-02-04	14:46:00.55	16.1935	-61.9573	176.30	3.40	0.50
17-02-06	18:21:55.94	16.2790	-61.0531	76.55	4.11	0.40
17-02-07	01:31:39.44	16.7929	-61.8421	13.11	2.84	0.47
17-02-07	11:41:20.02	16.7939	-61.8405	13.56	3.33	0.58
17-02-09	09:32:36.95	16.7373	-61.9979	110.90	3.57	0.42
17-02-11	03:46:46.20	17.8241	-61.5507	26.01	4.03	0.53
17-02-12	20:16:17.86	14.9929	-61.4668	190.12	3.61	0.47
17-02-14	14:02:56.90	17.1480	-61.5534	22.74	3.71	0.75
17-02-17	17:33:05.07	15.6766	-60.9620	76.13	3.03	0.28
17-02-18	10:18:33.89	15.6321	-60.6337	34.42	3.18	0.43
17-02-21	13:30:03.12	15.0838	-61.1920	148.12	3.10	0.39
17-02-21	20:10:05.61	17.5165	-62.0962	39.42	3.97	0.46
17-02-27	09:15:16.46	15.1628	-60.3875	45.55	3.38	0.51
17-02-28	02:40:57.90	17.5947	-61.8955	42.97	3.90	0.65
17-02-28	03:16:46.58	15.8521	-60.5973	44.62	3.28	0.55
17-03-02	15:03:11.25	17.5951	-61.8772	39.94	3.37	0.49
17-03-06	17:35:00.61	15.3531	-61.0708	133.98	3.81	0.48
17-03-07	00:06:57.30	17.3636	-62.5056	111.42	3.97	0.56
17-03-07	10:51:34.22	17.4214	-61.9075	38.88	3.40	0.52
17-03-10	06:01:17.60	17.5024	-62.7492	102.63	4.78	0.58
17-03-10	14:11:47.33	13.5232	-61.1266	133.82	3.49	0.30
17-03-10	20:19:32.41	11.2523	-60.7321	49.89	4.47	0.79
17-03-14	00:18:35.57	17.5054	-62.7546	105.29	4.44	0.50
17-03-19	17:32:07.00	18.0826	-61.4345	42.94	3.39	0.63
17-03-20	19:01:49.52	11.2822	-60.7476	47.63	4.87	1.00
17-03-20	20:58:47.99	14.7961	-61.2983	164.38	3.26	0.39
17-03-21	00:01:41.72	16.8004	-61.3324	47.34	3.18	0.64
17-03-21	21:59:14.84	15.0319	-61.2641	147.14	3.29	0.31
17-03-22	07:33:01.47	15.0045	-60.4810	44.06	3.41	0.48
17-03-25	14:46:33.14	11.2506	-60.8024	48.32	4.32	0.96
17-03-26	18:53:31.85	16.8234	-61.3364	20.81	3.71	0.61
17-03-27	22:12:13.88	16.1272	-61.9710	174.79	3.37	0.45
17-03-30	03:56:39.15	15.7539	-61.2079	91.29	3.23	0.38
17-03-30	05:32:24.30	17.4376	-60.5659	34.70	3.63	0.79
17-03-30	07:27:47.40	13.6522	-60.1382	68.44	3.04	0.48
17-03-30	18:59:58.36	17.3119	-62.9221	159.81	3.55	0.46
17-03-31	22:50:47.25	14.9080	-60.5579	60.35	4.05	0.41
17-04-01	20:22:07.51	15.0585	-60.4412	49.06	3.48	0.40
17-04-02	12:59:52.91	15.0697	-60.5383	52.83	3.64	0.53
17-04-07	00:39:19.47	14.9064	-61.2614	172.17	3.90	0.50
17-04-07	21:45:34.57	12.4290	-60.3496	60.04	4.65	0.71
17-04-08	06:14:03.79	15.7418	-61.4813	10.58	3.50	0.53
17-04-10	18:20:25.49	15.1594	-60.3134	37.04	3.65	0.54
17-04-10	18:39:14.89	15.8231	-61.6137	145.76	3.37	0.42
17-04-12	14:47:01.72	16.1043	-61.9085	169.09	3.51	0.41
17-04-13	00:44:53.40	16.1720	-61.1369	63.37	3.26	0.34
17-04-15	07:06:52.94	17.3324	-62.9312	143.29	3.18	0.46
17-04-15	18:16:17.98	17.5370	-61.0468	19.09	4.73	0.65
17-04-15	18:48:26.36	17.5312	-61.0848	20.77	3.67	0.71

17-04-16	10:10:32.08	17.5506	-61.0678	19.90	3.67	0.57
17-04-17	04:13:11.10	17.4934	-61.0537	14.74	4.23	0.46
17-04-17	06:25:11.40	17.5133	-61.0247	20.59	5.13	0.59
17-04-17	08:28:51.30	17.4893	-61.1148	14.38	3.93	0.81
17-04-17	15:12:00.58	17.4836	-61.0380	18.25	4.03	0.87
17-04-17	16:08:01.04	17.5323	-61.0562	14.55	3.92	0.73
17-04-19	20:32:03.41	17.5015	-61.0026	21.67	4.09	0.81
17-04-20	01:14:23.01	17.5382	-61.0183	21.25	3.63	1.02
17-04-20	22:22:10.34	17.5259	-61.0866	18.89	3.51	0.53
17-04-21	10:16:01.46	15.0438	-60.5065	54.42	4.41	0.39
17-04-22	03:29:27.75	14.0205	-60.1253	40.68	3.00	0.57
17-04-22	03:48:17.91	17.5250	-61.0571	17.76	3.86	0.63
17-04-22	09:13:53.49	17.5539	-61.0302	16.29	3.71	0.69
17-04-23	01:52:22.68	11.0106	-62.1931	98.09	4.97	0.96
17-04-23	14:04:03.80	13.6691	-59.5945	60.14	3.14	0.62
17-04-24	09:24:36.31	15.0268	-60.4966	48.07	3.65	0.67
17-04-24	22:21:07.33	17.5277	-61.0115	19.39	3.81	1.30
17-04-25	09:53:31.81	16.8355	-60.9151	15.71	4.57	0.78
17-04-27	20:42:48.71	15.8234	-61.5942	5.28	3.30	0.58
17-04-27	20:54:32.75	15.8281	-61.5925	4.28	3.26	0.54
17-04-27	22:57:09.40	15.8217	-61.5949	4.55	3.43	0.58
17-04-29	07:49:59.97	15.8385	-61.6026	4.59	2.85	0.42
17-04-29	13:32:03.02	15.8321	-61.6011	4.70	2.71	0.46
17-04-29	14:26:12.46	15.8298	-61.6056	4.00	3.01	0.51
17-04-29	14:54:26.20	15.8321	-61.6111	1.55	3.03	0.45
17-04-29	14:58:17.71	15.8318	-61.6150	0.41	2.81	0.35
17-04-30	09:49:12.87	15.0461	-60.4935	52.38	3.04	0.47
17-04-30	19:04:00.88	15.8283	-61.6081	4.30	3.31	0.84
17-04-30	23:13:12.85	15.8351	-61.6044	3.86	2.97	0.44
17-05-02	06:28:12.31	11.6675	-61.8544	145.30	4.06	0.54
17-05-05	20:03:19.93	14.8248	-61.0278	147.90	3.86	0.49
17-05-09	14:52:14.58	15.8249	-61.5668	6.54	2.94	0.51